Clim. Past Discuss., 2, 657–709, 2006
www.clim-past-discuss.net/2/657/2006/

Climate of the Past Discussions

Climate of the Past Discussions is the access reviewed discussion forum of *Climate of the Past*

Modelling ocean circulation, climate and oxygen isotopes in the ocean over the last 120 000 years

R. Marsh[1], M. P. L. M. Smith[1], E. J. Rohling[1], D. J. Lunt[2], T. M. Lenton[3,4], M. S. Williamson[3,4,*], and A. Yool[1]

[1]National Oceanography Centre, University of Southampton, UK
[2]Bristol Research Initiative for the Dynamic Global Environment (BRIDGE), School of Geographical Sciences, University of Bristol, UK
[3]School of Environmental Sciences, University of East Anglia, UK
[4]Tyndall Centre, University of East Anglia, UK
[*]now at: Quantum Information Group, University of Leeds, UK

Received: 25 August 2006 – Accepted: 29 August 2006 – Published: 4 September 2006

Correspondence to: R. Marsh (rma@noc.soton.ac.uk)

Abstract

A new Earth System Model of Intermediate Complexity, GENIE-1, is used to simulate the most recent glacial-interglacial cycle by prescribing orbital forcing, atmospheric CO_2 concentration, and the time evolution of ice sheet extent and orography. A series of experiments investigates uncertainty in the amplitude, frequency and location of prescribed meltwater pulses (MWPs) associated with Heinrich events in the North Atlantic and layers enriched in ice rafted debris around Antarctica. Associated with each MWP is a flux into the ocean of very light glacial oxygen isotope ratios, which serve as a tracer of the melt water. Additionally accounted for are temperature-related changes in the fractionation of stable oxygen isotopes between water and calcite. Modelled forwards from 120 000 years ago, simulated oxygen isotope records can thus be directly compared with measurements in calcite taken from International Marine Global Change Study (IMAGES) and Ocean Drilling Program (ODP) sediment cores at three locations representative of the North and South Atlantic, and the South Pacific. During the period of simulation corresponding to Marine Isotope Stage 3, the best agreement between the simulated oxygen isotope record in the North Atlantic and core measurements is found in the experiment that includes MWPs around Antarctica as well as into the North Atlantic. This challenges previous assumptions about the dominant role of northern ice sheets in glacial sea-level variability.

1 Introduction

The last 120 000 years span the most recent cycle of glaciation, between the last (Eemian) and current (Holocene) interglacial periods. The overall increase in ice sheet extent up to the Last Glacial Maximum (LGM) at around 21 ky Before Present (BP) was not steady. Glacial climate comprises a series of cold stadials and relatively warm interstadials spanning millennia, the Dansgaard-Oeschger (D-O) events (Dansgaard et al., 1993). D-O events are most evident in northern hemisphere ice-core records

between 75 and 20 kyr BP, and the associated transitions between stadial and interstadial climate are abrupt with respect to both their physical definition (Rahmstorf, 2000) and their timescale (Clark et al., 2002). Northern hemisphere temperature abruptly shifted by 6–10°C in mid to high latitudes (Broecker, 2000; Rahmstorf, 2003), initiating D-O interstadials which gently cooled and then rapidly collapsed into D-O stadials. The dominant periodicity is often about 1500 years between each D-O event, although there is evidence for periodicity at around 3000 years and 4500 years (Alley et al., 2001). These events are of global significance. For example, Voelker et al. (2002) observe the signature of D-O-style periodicity at 183 sites around the globe during 59–29 kyr BP (Marine Isotope Stage 3).

D-O cycles are thought to be northern hemisphere phenomena, but D-O-style climate variability has been observed beyond the northern hemisphere (Pahnke et al., 2003; Rohling et al., 2003). The timing of fluctuations in Antarctic ice-core records has been related to northern ice-core records by means of synchronisation of variations in atmospherically-derived methane concentrations measured in bubbles trapped within the ice (Blunier et al., 1998). This timing relationship has been confirmed by co-registered proxies in marine sediment records (Shackleton et al., 2000; Pahnke et al., 2003). Antarctic records follow a different "rhythm" than that of the northern hemisphere: they are chatcaterised by fewer, and more symmetric, climate fluctuations (Petit et al., 1999; Shackleton et al., 2000; Rohling et al., 2003). Furthermore, marine sediment records show a difference in oxygen isotope composition between planktonic (surface) and benthic (sea floor) foraminifera, suggesting that climate in the southern latitudes is closely related to ice volume, which in turn is analogous to sea level. Studies which have separated temperature and sea-level effects (Cutler et al., 2003), corroborated with independent sea level records, have shown that sea level may have varied by as much as 30 m. An independent study, based on Red Sea oxygen isotope data and hydraulic exchange theory (Siddall et al. 2003), suggests a similar amplitude of sea level variability.

Variation of sea level with a timing history similar to Antarctic climate fluctuations

may point to an importance of the Antarctic ice sheet in forcing global climate, although such an interpretation may be over-simplified. Knutti et al. (2004) simulate millennial rhythms in Antarctic air temperature variability which lead similar cycles of sea level associated with northern meltwater pulses. In the simulations this is due to a "thermal-freshwater seesaw", whereby the Southern Ocean (and Antarctic climate) responds on a millennial timescale to abrupt (decadal-timescale) changes in North Atlantic deep water formation that arise when prescribed freshening in the North Atlantic reaches a critical threshold. Hill et al. (2006) present proxy evidence for summer melting of the southern Laurentide ice sheet margin that is coincident with Antarctic warmings, suggesting the global importance of seasonality in ice sheet mass balance. Flückiger et al. (2006) use model simulations to demonstrate how modest freshwater input to the whole Atlantic (between 50° N and 70° N) can lead to abrupt reorganisation of the global ocean circulation and sufficient regional sea-level rise (through changes in local dynamic topography and thermal expansion of the global ocean) to destabilise the Laurentide ice sheet. This sequence of events amounts to a positive feedback, leading to more prolonged melting, sub-surface ocean warming and sea-level rise, on a millennial timescale. In spite of the range of explanations for millennial sea-level variability that centre on northern ice sheets, Rohling et al. (2004) show that the oxygen isotope record in sediment cores around the World Ocean is in fact more consistent with roughly equal meltwater contributions from both Antarctica and the northern ice sheets.

Episodic break-up of the northern ice sheets is suggested by "Heinrich events", recorded as layers in the sediment record which contain high percentages of lithic fragments (Heinrich, 1988). The lithic fragments originate in icebergs and are deposited to the sea floor as a result of melting of the encapsulating ice. The resulting coarse sedimentary component is termed ice-rafted detritus or debris (IRD). Extensive fieldwork has established high IRD percentages and high magnetic susceptibility in a mid-latitude area of the North Atlantic known as the IRD belt (Ruddiman, 1977; Hemming, 2004). Heinrich events tend to occur during the stadial phase of D-O cycles (Alley and Clark,

1999), followed by rapid warming (Bond et al., 1993). This interplay between Heinrich events and D-O cycles is not well understood, in terms of triggers and responses. While some IRD layers are linked to iceberg calving from circum-Atlantic ice sheets that are driven by D-O climate cycles, there are some suggestions that Heinrich events might occur independently of D-O cycles (Marshall and Koutnik, 2006).

Six Heinrich events were initially identified, in the last 100 kyr, labelled H1 through to H6 with increasing age from youngest to oldest. The most recent Younger Dryas (YD) stadial has been linked to an event analogous to H1–H6, labelled as H0 (Andrews et al., 1994). While H0 is not supported by massive IRD deposition, it is characterised by catastrophic drainage of proglacial lakes, most notably Lake Agassiz (Upham, 1895). Other studies have identified earlier Heinrich events, H7 and H9 (Chapman and Shackleton, 1998). Most Heinrich layers increase to a maximum thickness of around 50 cm in a band lying between the Grand Banks and the mid-Atlantic (Grousset et al., 1993; Andrews et al., 1994). Events H1-H6 have been further characterised by specific differences in the IRD layers which indicate two different origins. H1, H2, H4 and H5 have been defined as Hudson Strait (HS) Heinrich events (Bond et al., 1992; Broecker et al., 1992), analogous to the cemented marl definition proposed by Heinrich (1988) and further supported by four independent geochemical measurements (Hemming, 2004). H3 and H6 differ from the HS Heinrich events, as they only show a modest increase in the flux and number of lithic grains despite the high percentage of IRD (Hemming, 2004). It has been suggested that H3 and H6 were in fact low foraminiferal intervals rather than large IRD events, which would account for the high percentage of IRD as a result of a closed-sum or matrix effect in the data (Gwiazda et al., 1996). Also, the detritus appears to be derived from sources other than the HS events. Gwiazda et al. (1996) proposed that the sediment found in H3 and H6 were of European origin, which is supported by Grousset et al. (2000). Though some aspects of H3 suggest it may be of Hudson Strait origin (Grousset et al., 1993; Bond and Lotti, 1995), the spatial pattern of the IRD is dissimilar to that of the HS Heinrich events (Grousset et al., 1993). As well as any link between Heinrich events and D-O cycles, the processes

driving Heinrich events are also a matter of debate, although the leading hypothesis is glaciological instability which controls episodic purging of the Laurentide ice sheet – see Hemming (2004) for further discussion.

Even before Heinrich events and D-O cycles were formally characterised, Broecker et al. (1985) suggested that the associated abrupt changes in climate may be due to alterations in the oceanic themohaline circulation (THC). Palaeoceanographic proxies have since been used to reconstruct some aspects of the THC. For example, the relative age of deep water is traced by δ^{13}C. Alley and Clark (1999) have used the distribution of δ^{13}C from sediment cores in the eastern Atlantic basin to reconstruct the pattern of relative age at three time slices, indicating that largest alterations in the THC were due to three possible modes: Modern, Glacial and Heinrich. The differences between each mode are thought to lie in the formation of North Atlantic Deep Water (NADW); in the Modern mode, deep water is formed in the Nordic Seas and subsequently flows over the Greenland-Scotland ridge where it mixes and re-circulates with the water from the Labrador Sea to form NADW (Dickson and Brown, 1994). In the Glacial mode, no deep water was produced in the Nordic Seas, while open-ocean convection further to the south restricted NADW to the upper 2500 m (Labeyrie et al., 1992). Brine rejection under ice may have provided another mechanism of deep water formation in the Glacial mode (Sarnthein et al., 1994). The Heinrich mode is characterised by no significant production of NADW (McManus et al., 2004). Instead waters from the Antarctic may have penetrated the North Atlantic up to depths of 1000 m (Sarnthein et al., 1994). The Heinrich mode provides information on the mechanisms which affect the THC. The ice introduced as part of Heinrich events also injected large amounts of fresh water into the ocean system and this input of fresh water has been suggested as a key factor in forcing THC collapse (Broecker et al., 1985; 1988).

Much of the last glacial cycle has been dominated by the growth of large northern hemisphere ice sheets. Observational data have provided good constraints on the maximum ice extent at the LGM (Clark and Mix, 2002) as well as the history of their subsequent retreat. At the LGM the Northern Hemisphere contained a number of large

ice sheets: the Cordilleran, Laurentide, Innuitian, Greenland, British, Scandinavian, Barents Sea, and Kara Sea ice sheets. The Antarctic Ice Sheet may have changed substantially in the past as well. Reconstructions of its extent at the LGM show that it probably extended to the shelf edge around the majority of the continent (Anderson et al., 2002). However, the thickness and volume of these ice sheets and their evolution over time are much harder to reconstruct from geomorphological evidence and generally need to be inferred from indirect evidence and modelling (Zweck and Huybrechts, 2005).

Although there is a steady increase in the availability of sea-level reconstructions for the pre-LGM period of the last glacial cycle, these illustrate only total global ice volume and not the source contributions of the various individial ice sheets. The most direct measurements of global ice volume can be obtained via changes in global sea level derived from coral reef data (Bard et al., 1996), although other indirect methods have been developed (Shackleton et al., 1987; Rohling et al., 1998; Waelbroeck et al., 2002; Siddall et al., 2003). Another method is based on glacio-isostatic rebound models (Peltier, 2002; Milne et al., 2002), which use the adjustments of the geoid to predict area-integrated ice volumes and have predicted total ice sheet volume change since the LGM equivalent to sea level change in the range 115–135 m (Milne et al., 2002). Geomorphological data from before the LGM are scarce, because the record was mostly destroyed by the maximum advance during the LGM.

While the Laurentide ice sheet is identified as the most likely source of meltwater that impacted the Atlantic THC and climate and has thus become a focus of attention (Broecker et al., 1985, 1988), there has been little consideration of variations in the Antarctic ice sheet. The Antarctic ice sheet is often regarded as highly stable (Ganopolski and Rahmstorf, 2001), but recent studies may suggest otherwise. Kanfoush et al. (2000, 2002) identify the distinct presence of IRD peaks in Southern Ocean sediment cores. Clark et al. (2002) and Weaver et al. (2003) argue that a 20 m sea-level rise in approximately 500 years during the last deglaciation may have been due to an Antarctic meltwater pulse. Recent model studies have further disputed that the

Antarctic ice sheet is relatively stable and did not contribute large volumes of freshwater (Weaver et al., 2003; Stocker and Johnsen, 2003; Rohling et al., 2004).

Paleoclimate records provide a snapshot of past climate at discrete locations, and have demonstrated the presence of large and abrupt regime change. However there is a need to extend such quasi-local records into a global context. This can be done using appropriate models of the earth system. Incorporating full dynamics, coupled ocean-atmosphere general circulation models (OAGCMs) have been used extensively in paleoclimate studies, although their use is restricted by computational cost to equilibrium or short transient simulations of no more than a few thousand years. For longer simulations, Earth system Models of Intermediate Complexity (EMICs) have proved useful (Claussen et al., 2002). Furthermore, the transfer functions used to link climate proxy data (such as oxygen isotopes) to physical climate variables (such as temperature) are commonly based on assumptions about the Earth system that do not account for many processes which cause deviation from equilibrium fractionation. To enhance our interpretation of the proxy records, it is necessary to engage in forward modelling of climate proxies.

Atmospheric circulation models have been modified to include the atmospheric cycling of oxygen isotopes, and to infer the sea surface distribution of the oxygen isotope ratio, δ^{18}O, based on modelled evaporative fluxes and precipitation (Jouzel et al., 1987; Juillet-Leclerc et al., 1997). Moreover, modelling of δ^{18}O has been incorporated into oceanic general circulation models (Schmidt, 1998), the forward modelled distribution of δ^{18}O has been coupled with a simple ecological model (Schmidt, 1999), and ocean models have been evaluated in terms of δ^{18}O-salinity relationships (Delaygue et al., 2000). However, the modelling of oxygen isotopes in coupled atmosphere-ocean models is in its infancy. In the only such studies to our knowledge, the CLIMBER-2 EMIC has been used to simulate ocean δ^{18}O content under modern and LGM climate (Roche et al., 2004a), and to establish the duration and freshwater release of Heinrich event 4 (Roche et al., 2004b).

In the present study, we carry out a number of simulations of the last glacial-

interglacial cycle with an EMIC forced with time-varying insolation (according to orbital parameters), atmospheric CO_2 concentration, and ice sheets (extent and orography). To our knowledge, this is the first time that a model of such complexity has been used to simulate a full glacial-interglacial cycle. Previously, experiments of such length have been restricted to somewhat lower complexity. For example, Gallee et al. (1991) used a coupled sectorially-averaged climate-ice sheet model to simulate the last glacial cycle, while Marshall and Koutnik (2006) force a more complex ice sheet model with reconstructed boundary conditions to simulate iceberg fluxes at the centennial timescale.

The present paper is arranged as follows. First we describe the GENIE-1 EMIC, followed by details of experimental design (boundary conditions, meltwater pulses and δ^{18}O forcing). Model results are presented in terms of high latitude climate (for evaluation against ice core data), variability of the thermohaline circulation, and changes in the ocean temperature and δ^{18}O (in both water and calcite). We conclude with a discussion of the results obtained here alongside δ^{18}O measurements in calcite from sediment cores, to shed light on the relative contribution of fluctuations in northern and southern hemisphere ice sheets to variability of glacial sea level and climate.

2 The model

We use the GENIE-1 EMIC, developed through the Grid ENabled Integrated Earth system modelling (GENIE) project (http://www.genie.ac.uk). At the core of GENIE-1 is an ocean-atmosphere-sea ice climate model, previously known as C-GOLDSTEIN and described in Edwards and Marsh (2005). In addition, we use a new land surface physics scheme, the Efficient Numerical Terrestrial Scheme (ENTS) of Williamson et al. (2006). GENIE-1 has been designed for computational speed, to enable multi-millennial transient paleo-simulations and long-term future projections. Around 4000 years of model integration is achieved in 1 CPU hour on a single 64-bit processor. In the spectrum of model complexity (Claussen et al., 2002), GENIE-1 has dimensionality equivalent to the UVic Earth System Model (Weaver et al., 2001). Below we outline the

structure of model components and the importance of key parameters.

2.1 Ocean and sea ice

The frictional geostrophic ocean, GOLDSTEIN, is three dimensional and is more efficient than 3-D global ocean models based on the primitive equations, due to the exclusion of momentum advection and acceleration. The model has eight depth levels on a uniformly logarithmic grid, with spacing increasing as a function of depth from 175 m to 1420 m with a maximum depth of 5 km. The horizontal grid comprises equal-area grid-boxes of constant dimensions 10° in longitude and sin(π/36) in sin(latitude). Despite this low horizontal and vertical resolution, the main features of global ocean topography are captured – see Fig. 1. The land-sea mask, and ocean topography, is maintained as for the present day throughout the experiments. In previous paleoclimate experiments with C-GOLDSTEIN, of relatively short duration, the Bering Strait was closed (Rohling et al., 2004). Changing the land-sea mask and ocean topography during long transient experiment would demand careful adjustment of ocean temperature and salinity to ensure conservation of heat and freshwater within the model as a whole.

The model also features a dynamic and thermodynamic sea-ice component (Edwards and Marsh, 2005). Sea ice thermodynamics is based on the schemes originally proposed by Semtner (1976) and Hibler (1979), whereby thermodynamic growth and decay of sea ice is dependent upon the net heat flux into the ice from both the ocean and the atmosphere. The sea ice dynamics are simple and are governed by advection due to surface currents and some horizontal diffusion.

2.2 Atmosphere

The atmosphere is a 2-D energy moisture balance model (EMBM) based on an original development of Fanning and Weaver (1996) and Weaver et al. (2001), as described in detail in Edwards and Marsh (2005). However, Lenton et al. (2006) introduced a number of changes: seasonality of insolation; separation of surface and atmosphere/cloud

albedo; inclusion of a relaxation time for precipitation; time-varying wind forcing (specifying monthly climatological present-day winds).

2.3 Land surface

Land topography is based on the Fourier-filtered interpolation of ETOPO5 observationally derived data (Edwards and Marsh, 2005). The new ENTS land surface scheme includes a minimal representation of land surface physics and hydrology for use in a spatially resolved context. Here, the land model is run with a fixed vegetation pattern: the equilibrium annual-mean distribution at the end of a pre-industrial simulation. The vegetation scheme determines the land roughness length and also the surface albedo. Terrestrial ice sheets are prescribed in extent and orography, but may vary in time. Around ice sheet margins, the fixed vegetation is interpolated as the ice sheet grows and shrinks, dependent upon the fraction of ice present in the grid cell.

2.4 Parameter sets

The model was run with two different parameter sets – "subjective" and "traceable" – to test the robustness of model results and link the present study to previous studies. "Subjective" parameter sets are obtained using the common procedure of altering a single parameter in a sequence of experiments to improve the qualitative agreement with chosen data (Lenton et al., 2006). Subjective tuning is somewhat limited, as parameters are only varied individually and multi-dimensional parameter space cannot be thoroughly explored. In contrast, the traceable parameter set is obtained using the Ensemble Kalman Filter (Hargreaves et al., 2004). This is a sophisticated sequential data assimilation method which provides an efficient computational (recursive) means to estimate the state of a process governed by several parameters, in a way that minimizes the mean of the squared error and is set to keep within bounds of both prior beliefs and actual climate observations. Both parameter sets were tuned using present-day climate observations. The parameter sets are listed in Table 1 and discussed here in

terms of their influence on the ocean, sea ice, and atmosphere. The individual parameters are discussed at greater length in Lenton et al. (2006).

In the ocean, isopycnal diffusivity (κ_h) and diapycnal diffusivity (κ_v) control mixing and transport in the horizontal and vertical planes respectively, and are important for ocean circulation, especially the thermohaline circulation and its response to freshwater perturbations. The momentum drag (Rayleigh friction) coefficient (λ) is a frictional timescale, while a scaling factor (W) artificially increases wind stress to obtain more realistic wind-driven gyres and Antarctic Circumpolar Current (which are otherwise strongly retarded by friction). Suitable choice of the lateral diffusivity of ice thickness and ice concentration (κ_i) ensures that sea ice does not grow too thick in regions of formation, especially in the Arctic.

In the atmosphere, meridional gradients of air temperature and humidity are controlled by heat and moisture diffusivity. Heat diffusivity is prescribed as a latitude-dependent function, which peaks at the equator, with amplitude defined by κ_T, and decreases to a non-zero minimum at the North Pole and zero at the South Pole. The shape of this peaked function is controlled by two further parameters: a length scale (l_d) which defines the sharpness of the equatorial peak, and a slope (s_d) which defines the north-south asymmetry of heat diffusivity. Moisture diffusivity (κ_q) is constant across all latitudes. Two further parameters are used to scale zonal advective transport of heat (β_T) and the meridonal and zonal transport of moisture (β_q) by winds. Advective transports can improve global patterns of temperature and humidity. An additional flux correction (F_a) is applied to the surface freshwater flux in the Atlantic (net evaporation) and Pacific (net precipitation), to mimick an additional atmospheric moisture transport between the basins. This is necessary to maintain an Atlantic-Pacific surface salinity contrast that is sufficient for "Conveyor mode" operation of the global thermohaline circulation. It should be noted that this is not a flux correction in terms of correcting climatic drift. Two further parameters ($r_{\max}$ and τ_{pptn}) are used to modify the parameterization of precipitation (see Lenton et al., 2006), specifically to improve continental precipitation rates.

3 Experimental design

For the GENIE-1 experiments, we developed glacial-interglacial boundary conditions, a set of meltwater pulse scenarios, and a scheme for $\delta^{18}O$ forcing. Details are outlined in Sects. 3.1–3.3 below. Results from model experiments were selected at locations where we have reliable measurements of climate over the last glacial cycle. We recorded surface air temperatures in gridboxes coincident with the GISP2 (72°36′ N, 38°30′ W) and Vostok (78°27′ S, 106°51′ E) ice core sites. We also saved surface and bottom values of $\delta^{18}O$ and temperature in gridboxes coincident with three well-studied sediment cores: the Iberian Margin, North Atlantic at 37°48′ N, 10°10′ W (Sediment Core MD95-2042, Shackleton et al., 2000); Bouvet Island, Atlantic sector of Southern Ocean at 53.2° S, 05.1° E (Sediment Core ODP 1094, Kanfoush et al., 2002); Chatham Rise, Pacific sector of Southern Ocean at 45°32 S, 174°55 E (Sediment Core MD97-2120, Pahnke et al., 2003).

3.1 Boundary conditions, initialisation and spin-up

The time-varying boundary conditions comprise orbital forcing of insolation, atmospheric CO_2, and reconstructed ice sheet extent and orography. In addition, we experiment with three scenarios of meltwater pulses (MWPs), prescribing the amplitude, timing and location according to published evidence and some basic hypotheses. According to a simple glacial-interglacial sea-level cycle and the prescribed MWPs, we include corresponding surface forcing of $\delta^{18}O$.

3.1.1 Orbital forcing

Solar insolation changes with variations in the Earth's orbit, which are caused by gravitational interaction between the sun, the planets and their satellites (Pälike, 2005). Consequently the amount of energy received at a given latitude is dependent upon the Earth's orbital and rotational parameters defined as obliquity, eccentricity, and pre-

cession, which vary on several dominant time scales, including, ∼20 Kyr (precession), ∼40 Kyr (obliquity) and ∼100 and 400 Kyr (eccentricity). Obliquity variations have a substantial effect on local annual-mean insolation but do not influence the global mean annual incoming solar radiation. Eccentricity variations do affect annual insolation, although the effect is relatively small. Variations in precession control the timing of the approach of the perihelion (when the Earth is closest to the Sun) and consequently the seasonality of insolation. The model uses the orbital parameters shown in Fig. 2, to generate the insolation forcing as a function of latitude. These parameters are constructed using data from Berger (1978).

3.1.2 Atmospheric CO_2

Ice core records have shown that that CO_2 is an important amplifier of orbital forcing (Genthon et al., 1987). We use the record of CO_2 directly measured in air bubbles trapped in a Vostok ice core (Petit et al., 1999), interpolated to every 1000 years, shown in Fig. 3a. The CO_2 concentrations are set to the GT4 timescale (Petit et al., 1999), an extension of an original timescale (Lorius et al. 1985) and including subsequent improvements (Jouzel et al., 1993). The chronology is derived from ice-flow and ice accumulation models and therefore is purely based on physics rather than climatic correlations, apart from a number of control ages. The timescale accuracy of the CO_2 reconstruction over the last 120 ky is ±5 ky for the last 110 ky, decreasing to ±10 ky for the remaining 10 ky. The Vostok record clearly indicates the approximate 100 ppmv glacial-interglacial range in atmospheric CO_2, with minimum values around the LGM.

3.1.3 Ice sheet extent and orography

The ICE-4G reconstruction has provided terrestrial ice sheet fraction and orography for the period 21 ky BP to the present (Peltier, 1994). The ICE-4G method is based on an understanding of how relative sea-level records the viscous deformation of the earth, due to the presence of terrestrial ice sheets. The ICE-4G reconstruction uses the

exponential relaxation curves of ice covered regions. These curves contain information about the internal rhelogy of the planet and the space- and time-dependent thickness of the ice load when this is combined with relative sea-level data, and are deconvoluted to produce the paleotopography of the terrestrial ice sheets.

In a related GENIE-1 study, Lunt et al. (2006) use the ICE-4G reconstructions every 1000 years over 0–21 ky BP, along with the Arnold et al. (2002) reconstruction of northern ice sheets at 30 ky BP, and combine the ICE-4G data over 0–21 ky BP and the Vostok δ^{18}O record (Petit et al., 1999) over 0–29 ky BP to obtain ice sheet extent and orography over 22–29 ky BP. As the ICE-4G record spans the period of maximum ice cover (LGM) to the present, which can be assumed as an approximation of the minimum amount of ice cover over the glacial-interglacial cycle (neglecting the Greenland ice sheet), this period can be further used as an analogue of the ice volume change during the period 31–120 ky BP. In the present study, we therefore extend the millennial time series of ice sheet extent and orography back over 31–120 ky BP using the sea level reconstruction of Siddall et al. (2003) shown in Fig. 3b, as an indirect measure of change in global ice volume. The reconstruction spans +8.1 m to –112.4 m, relative to present day sea level. Figure 4 shows ice sheet extent and orography every 5000 years over 35–10 ky BP, illustrating growth of ice sheets up to the LGM (around 20 ky BP) and the subsequent deglaciation. Use of reconstructed sea level leads to pre-30 ky BP ice sheets of somewhat limited extent. While this may be inconsistent with other proxy evidence, the precise details of reconstructed ice sheets are of secondary importance in the present study, and in the absence of more quantitative information we regard our reconstruction as adequate for present purposes. Similar methods have been used to reconstruct forcing for other glacial-interglacial model studies. In order to force an ice sheet model over the last glacial cycle, Marshall and Koutnik (2006) generate precipitation and temperature fields every 100 years by interpolating between LGM and present-day GCM simulations according to a "glacial index" derived from the GISP2 ice core δ^{18}O stratigraphy.

3.1.4 Initialisation and spin-up

The ocean and atmosphere are initially at rest and prognostic variables are set to constant values: the ocean with temperature 20°C and salinity 34.9 psu; the atmosphere with temperature 0°C and relative humidity 0%. Each experiment is of duration 124 000 years. For the first 4000 years, boundary conditions are fixed at values for 120 ky BP in order for the thermohaline circulation and global climate to reach an equilibrium state. Lunt et al. (2006) find that this is sufficient time for a transient run to come to equilibrium, and that transient simulations are not very far removed from their equivalent equilibrium simulation. The implication is that, if we had started from, say, 150 ky BP and carried out a 30-ky spin-up under transient boundary conditions for 150–120 ky BP, we would obtain a very similar initial state.

3.2 Meltwater pulses

Our experiments are forced using prescribed meltwater pulses (MWP) to test the model sensitivity and uncertainties in the amplitude, frequency and location of the prescribed MWP. Our choices of chronology, duration, location and magnitude of MWPs are outlined below, followed by a description of the three MWP scenarios.

3.2.1 Chronology of prescribed Heinrich events

Our MWP chronology is determined from an analysis of the GISP2 non-sea-salt (nss) ion series, used to constrain the timing of Heinrich events during the most recent glaciation (Rohling et al., 2003). In this analysis, statistical significance tests were used to identify the strongest significant peaks coincident in time series of three nss ions: K^+, Ca^{2+} and Mg^{2+}. Peaks in the nss ion series correspond to alterations of the extent and intensity of polar circulation, which is considered to provide broader information on the climate system rather than a single climate indicator such as a proxy for local temperature (Rohling et al., 2003).

The prominent peaks in the ion series were considered also in terms of other published data (see Fig. 3 in Rohling et al., 2003). It is on this basis that we chose to use the ion series peaks, which correspond with Heinrich events indicated by the majority of other paleodata. Nine MWPs were subsequently chosen (Table 2). The majority of MWPs (corresponding to H0–H5) take place over 10–50 ky BP. Despite a number of significant peaks in the ion record before 50 ky BP, only three further MWPs were chosen (H6, H7 and H9), due to a lack of corroborating evidence. We note with caution that the number of sources supporting H6, H7 and H9 is considerably smaller than for H0–H5. The timing of each MWP is set to the nearest 500 years (from the dated nss ion peak), in accordance with our forcing scheme (updating MWP forcing at 500-year intervals) and consistent with the uncertainty in dating.

3.2.2 Duration of MWPs

The duration of northern MWPs is based on the most recent estimate of 495 ±255 years (Hemming, 2004). This estimate was ascertained via the synthesis of various techniques including the difference in ^{14}C ages across IRD layers, principally at H1 and H2, planktonic δ^{18}O age records, and sediment flux records from the ^{230}Th$_{excess}$ method. In the first instance, northern MWPs are applied as a 500-year increase to a prescribed magnitude (Sect. 3.2.4), followed by a 500-year decrease to zero. Of six Antarctic MWPs, two are of northern duration, while four are of 2000-year duration, the latter comprising 1000-year increases and decreases. We prescribe longer-duration southern MWPs as coincident with the four Antarctic warming events A1-A4 (Rohling et al., 2004).

3.2.3 Location of MWPs and background deglaciation flux

On the basis of field evidence for Heinrich events in the mid-latitude North Atlantic (Hemming, 2004), and following previous model experiments (e.g., Manabe and Stouffer, 1997), we apply MWPs equally at all ocean gridpoints in the Atlantic zone 50–70° N.

While debate surrounds the possibility of alternative routing of melt waters to lower latitudes or even the North Pacific (e.g., Broecker, 2006), we have not considered either alternative scenario here. As less is known about the origin of MWPs in the Southern Ocean, we apply these events equally at all ocean gridpoints adjacent to Antarctica. A background deglaciation flux is specified in the Atlantic zone 50–70° N in all cases.

3.2.4 Amplitude of MWPs

We choose different magnitudes for individual MWPs, in line with published estimates and uncertainty (Hemming, 2004). The amplitude of each MWP in our initial scenario (Sect. 3.2.5) is consistent with an estimated total volume, per typical Heinrich event, of 1×10^7 km^3 (Hemming, 2004). This estimate is based on a typical Heinrich IRD layer, combined with volume mapping of IRD layers across the North Atlantic during a typical Heinrich event, to derive the average volume of IRD. This volume is converted to a water volume using corrected δ^{18}O excursions and estimated δ^{18}O values of the Northern hemisphere glacial ice, adjusted to account for effects of the ocean circulation (Hemming, 2004). Based on this total volume, each MWP in our initial scenario corresponds to a peak freshwater flux of 0.3 Sv. A background deglaciation meltwater flux is also prescribed, corresponding (apart from MWP contributions during deglaciation) to a post-LGM sea level rise of 128 m.

3.2.5 Three MWP scenarios

Experiments MWP-1t (traceable parameter set) and MWP-1s (subjective parameter set) both feature the regime of MWPs shown in Fig. 5a: MWPs of moderate magnitude (0.3 Sv) and a strong background deglaciation over 10–21 ky BP. The deglaciation meltwater flux is highly idealised, lasting 10.5 kyr with a rapid 500-year onset at 20.5 ky BP, to a continued freshwater input of 0.15 Sv and followed by a rapid 500-year termination at 10 ky BP. MWPs specified during deglaciation are additional to the background meltwater flux.

Experiment MWP-2 (Fig. 5b) features a MWP regime corresponding to variable-sized Heinrich events plus two stronger deglaciation MWPs, and an intermediate-strength deglaciation flux. The total volume of meltwater released by the nine MWPs in MWP-2 is the same as in experiments MWP-1t and MWP1s. The Heinrich layer thicknesses (see Tables 1 and 3 in Hemming, 2004) from the cores that have been studied in or close to the IRD belt and IRD volume (Table 5 in Hemming, 2004) are used as a first order approximation for the two sizes of MWP. Using this approach, it was deemed that H0, H1, H2, H4 and H5 were major meltwater events and were assigned an amplitude of 0.48 Sv. Using a box model of Great Lakes hydrology constrained by oxygen isotope measurements, Moore et al. (2000) estimated outflow rates of around 0.1 Sv during the Younger Dryas. If sustained for the entire Younger Dryas, such an outflow rate would supply 130 Sv years of melt water. This is rather less than the total 240 Sv years supplied by our stronger prescribed MWP at H0, which supposes that other proglacial lakes also drained at this time. H3, H6, H7 and H9 are deemed minor events in comparison, and are attributed with an amplitude of 0.17 Sv. Due to the increased size of H0 and H1, the background deglaciation flux is reduced to 0.13 Sv.

Experiment MWP-3 (Fig. 5c) features a MWP regime consisting of the same variable sized Heinrich events as MWP-2, but with additional southern MWPs and a yet weaker background deglaciation (due to one southern MWP during deglaciation). Four identical southern MWPs are prescribed at 40, 46, 56 and 60 ky BP, corresponding to Antarctic warming events A1-A4 (Rohling et al., 2004). The events A1, A2 and A4 broadly coincide with the Heinrich events H4, H5 and H6 and in the absence of clearly documented phase relationships between northern and southern meltwater releases, the MWPs are specified to be synchronous. In contrast to the northern MWPs, these four southern MWPs are prescribed with duration of 2000 years and amplitude 0.25 Sv (for approximate parity with the stronger northern MWPs). We specify two further southern MWPs which are identical in size and duration to the major northern MWPs. The MWP at 14.5 ky BP is analogous to Meltwater Pulse 1A (MWP-1A), which may be of Antarctic origin (Clark et al., 2002). A MWP identical to that of 14.5 ky BP

is chosen at 53 ky BP to correspond with Southern Atlantic Event 5 (SA5) identified by Kanfoush et al. (2000). This particular event is included because it does not coincide with any northern MWPs, and is large in magnitude in comparison to the other SA events. As the additional southern MWP corresponding to MWP-1A accounts yet further for the deglacial melting, the background deglaciation flux in scenario MWP-3 is further reduced to 0.08 Sv.

3.3 Forcing oxygen isotope ratios

We henceforth distiguish between $\delta^{18}O$ in glacial meltwater ($\delta^{18}O_{glacial}$), ocean water ($\delta^{18}O_{water}$), and preserved in calcite ($\delta^{18}O_{calcite}$). MWPs are assigned a "signature" $\delta^{18}O_{glacial}$ value of –30‰ which remains constant through all experiments. Under the observed glacial-interglacial sea level change and MWP scenarios (Sect. 3.2.5), this choice of $\delta^{18}O_{glacial}$ allows us to reproduce the observed, approximate, increase of 2‰ in $\delta^{18}O_{calcite}$ (Sect. 4.3). The background value of $\delta^{18}O_{water}$ is initialised at zero everywhere. This accounts for an offset seen between the simulated sediment record and the observed sediment record (Sect. 4.3). This initial condition is unrealistic given the spatial variations in $\delta^{18}O_{water}$ due to fractionation on evaporation and sea ice melting/freezing, and varying $\delta^{18}O$ signatures in precipitation and runoff. As the full water isotope cycle is not yet represented in GENIE-1, these background effects are neglected in the present study. Our $\delta^{18}O_{calcite}$ reconstructions therefore are indicative only of relative changes, while the absolute values are not representative.

Simple implicit surface forcing of $\delta^{18}O_{water}$ is used. An evaporative flux is specified at every ocean gridpoint in the absence of MWP events during the period 20.5–120 ky BP ("non-MWP" forcing). This flux, also derived iteratively, ensures that the mean ocean $\delta^{18}O_{water}$ returns to the initial (120 ky BP) value at Present Day (nominally zero). The evaporative flux in MWP-1t, MWP-1s and MWP-2 (northern MWPs) is –0.028 Sv. The evaporative flux in MWP-3 (northern and southern MWPs) is –0.041 Sv. The larger evaporative flux in MWP-3 is necessary to account for the extra melting and hence

additional re-glaciation of the Antarctic ice sheet.

The flux of $\delta^{18}O_{water}$ at the ocean interface is constrained as follows:

$$\text{non – MWP case :} \quad \text{flux}(\delta^{18}O_{water}) = -\delta^{18}O_{glacial} \times \text{Evaporative flux} \tag{1}$$

$$\text{MWP case :} \quad \text{flux}(\delta^{18}O_{water}) = -\delta^{18}O_{glacial} \times \text{MWP flux} \tag{2}$$

The non-MWP $\delta^{18}O$ fluxes are applied equally at every ocean grid box. As for freshwater, MWP $\delta^{18}O$ fluxes are applied equally at Atlantic gridboxes in the region 50–70° N and equally at every gridbox adjacent to Antarctica. The sign convention for fluxes is positive upwards. Hence, as the evaporative flux is negative, the non-MWP $\delta^{18}O$ flux is positive, implying increase of $\delta^{18}O_{water}$. This mimics the gain of $H_2^{18}O$ through to preferential accumulation of $H_2^{16}O$ in ice sheets via the Rayleigh distillation process. The MWP flux of $\delta^{18}O$ is conversely negative, lowering oceanic $\delta^{18}O_{water}$ by mimicking the input of isotopically light meltwater.

4 Results

We present the following results: an evaluation of the simulated climate variability at high latitudes; the response of the thermohaline circulation to the applied forcing; $\delta^{18}O_{water}$, temperature, and reconstructed $\delta^{18}O_{calcite}$ time series, at the three core sites.

4.1 High latitude air temperature

Figure 6 shows time series of annual-mean air temperature simulated in the four GENIE-1 experiments (red, green, light blue and dark blue curves) for gridboxes closest to the GISP2 and Vostok drilling sites. Plotted alongside these (black curves) are air temperatures inferred from measurements of $\delta^{18}O$ at GISP2 (Alley, 2004) and at Vostok (Petit et al., 1999).

At the GISP2 site (Fig. 6a), the model is biased warm: in the present day by 2°C (with subjective parameters) to 5°C (with traceable parameters); under glacial climate by 10–15°C. These systematic differences are unsurprising given the very low meridional resolution at high latitudes (see Fig. 1) and the large uncertainty in ice sheet extent and orography prior to the LGM. In contrast, the GISP2 "Present Day minus LGM" temperature difference in both reconstruction and simulations is in the range 15–20°C. However, the strong millennial variability at the GISP2 site is not well simulated. Associated with each MWP is cooling at the GISP2 site by 3°C (with traceable parameters) or 5°C (with subjective parameters), considerably less than the abrupt changes of up to 15°C in the reconstructed record.

At the Vostok site (Fig. 6b), there is a warm bias of around 10°C with the traceable parameter set, while air temperatures obtained with the subjective parameter set are close to the reconstruction throughout. Although the simulated glacial-interglacial variability in air temperature compares well with the reconstructed record after 80 ky BP, agreement deteriorates considerably over 80–120 ky BP. This may be because the reconstructed sea level record of Siddall et al. (2003) is a better proxy for the volume and orography of the Antarctic ice sheet after around 80 ky BP, and that the largest changes in global ice volume take place in the northern hemisphere prior to 80 ky BP. We also note that millennial cooling events simulated at around 40 ky BP and 46 ky BP can be associated with similar amplitude events (though of longer duration) in the reconstructed record. Comparing simulated high-latitude air temperatures with the reconstructions, we retain the subjective parameter set for experiments MWP-2 and MWP-3, due to warm bias with the traceable parameter set.

4.2 Thermohaline circulation

The thermohaline circulation is largely characterised by the meridional overturning circulation (MOC). Figure 7 shows Global, Atlantic and Pacific meridional streamfunctions at the end of experiments MWP-1t and MWP-1s. In both experiments, the global thermohaline circulation is correctly in the "Conveyor" mode, with northern sinking and

inter-hemispheric southward flow of deep water in the Atlantic sector, and an opposite pattern of northward transport of deep water across the Equator and northern upwelling in the Pacific sector. There are, however, large differences in the strength and structure of the overturning cells. With the traceable parameter set, northern sinking and equatorial southward deep water transport in the Atlantic sector (Fig. 7c) amount to 17.7 Sv and 14.4 Sv respectively, compared to 26.4 Sv and 15.8 Sv with the subjective parameter set (Fig. 7d). Larger differences between the experiments are found in the Southern Ocean (Figs. 7a, b) and the Pacific (Figs. 7e, f). With the traceable (subjective) parameter set, we obtain 17.0 (37.2) Sv of downwelling in the Southern Ocean, largely balanced by 17.8 (27.6) Sv of upwelling in the Pacific sector (in both cases excluding shallow cells, in the upper 700 m). The downwelling and upwelling of deep waters in the Southern Ocean and Pacific sector with the subjective parameter set is about twice as strong as with the traceable parameter set, and in closer agreement with recent inverse estimates (e.g., Fig. 13 of Sloyan and Rintoul, 2001).

Figure 8 shows time series of maximum and minimum Atlantic overturning rates (Figs. 8a, b) and minimum Pacific overturning rate (Fig. 8c). The maximum time series measures the strength of northern sinking, while the two minimum time series measure the strength of southern sinking. The Atlantic Conveyor strength initially reaches 20 Sv (traceable parameters) and 28 Sv (subjective parameters). Aside from the strong millennial-timescale events, the background strength varies slightly under the transient boundary conditions: increasing by up to 2 Sv, around 20–30 ky BP and 85–90 ky BP (traceable parameters); decreasing by up to 2 Sv at 20 ky BP (subjective parameters). The reasons for these opposite responses to the forcing is unclear, although we note that the maximum overturning rate is located further north in experiment MWP-1s (50° N) compared to experiment MWP-1t (25° N) in Figs. 7c, d. Given that the effect of glacial boundary conditions is to shift climatic zones southwards, we might expect a more adverse effect (of global cooling) on Atlantic overturning strength with the subjective parameter set, as the deep sinking site is located further north. Critical evaluation of differences in the response of overturning rates to LGM forcing in

MWP-1t and MWP-1s is limited by our incomplete understanding of the glacial overturning circulation. While proxies suggest that the North Atlantic overturning at the LGM was weaker than during the Holocene (Duplessy et al., 1988), coupled models often simulate somewhat stronger overturning rates under LGM boundary conditions compared to Present Day control experiments (Kitoh et al., 2001; Hewitt et al., 2001), although the reasons for this strengthening differ from model to model: e.g., Kitoh et al. (2001) find stronger surface cooling adjacent to sea ice, while Hewitt et al. (2001) identify stronger, drier winds in mid-latitudes.

A major difference between MWP-1t and MWP-1s is seen during deglaciation. With the traceable parameter set, the Atlantic overturning collapses at 20 ky BP at the onset of the "background" deglaciation meltwater pulse (0.15 Sv), and remains collapsed until this pulse stops at 10 ky BP. In contrast, with the subjective parameter set the Atlantic overturning weakens from 26 Sv to 20 Sv at 20 ky BP and remains at this strength until 10 ky BP except for two brief collapses during additional meltwater forcing at 17 ky and 12.5 ky BP. We conclude that in multi-parameter space, there is an on/off threshold in the MOC response to freshwater forcing at the MWP-1 background deglaciation level. Given that the MOC is not believed to have collapsed throughout the entire deglaciation (McManus et al., 2004), we again prefer the subjective parameter set.

In all experiments, the maximum Atlantic overturning rate responds rapidly to MWP forcing. With the collapse of northern sinking, an opposite cell is quickly established, evident in excursions of the minimum Atlantic overturning rate of up to –10 Sv. In contrast, the Pacific overturning cell is little affected by MWP forcing, declining in strength by no more than 4 Sv in extreme cases. The response of Atlantic overturning strength to individual MWPs is shown in Fig. 9 by grouping together the responses to MWP-1 events in the experiments with traceable and subjective parameter sets, synchronised in time (so that initial weakening starts at year 100 in each case) and on an expanded time axis. With the traceable parameter set, collapse of the Atlantic overturning is rapid (MOC declines to half of initial strength around 200 years after onset of weakening) and complete only 400 years after the first weakening. Full recovery is not established until

1000 years afterwards. In comparison, collapse is somewhat slower with the subjective parameter set (initial strength is halved 400 years after initial weakening), and full recovery is established around 200 years earlier. We conclude that the thermohaline circulation is monostable in both experiments, but more strongly stable (in the Conveyor state) with the subjective parameter set. Stability of the thermohaline circulation is relevant for the spreading of meltwater and the associated $\delta^{18}O_{water}$ tracer at the millennial timescale.

4.3 Oxygen isotopes and temperature at the core sites

Measurements of $\delta^{18}O_{calcite}$ are obtained from both pelagic (planktonic) forams (Bouvet Island, Chatham Rise) and benthic forams (Iberian Margin). We therefore consider surface or bottom $\delta^{18}O_{water}$ and temperatures at each core site. Figure 10 shows time series of $\delta^{18}O_{water}$ in gridboxes closest to the three sediment cores, in bottom water (Iberia) and surface waters (Bouvet, Chatham). Based on our simple prescription of surface enrichment in $H_2^{18}O$ through preferential evaporation of $H_2^{16}O$ (Eq. 1), $\delta^{18}O_{water}$ increases throughout the global ocean between MWPs. A small discrepancy between the iterative routine used to construct and balance MWP and $\delta^{18}O$ fluxes over a glacial-interglacial cycle (Sect. 3.3) and the way that GENIE-1 time-interpolates this forcing causes the mean ocean $\delta^{18}O_{calcite}$ value to return to slightly positive values after the deglaciation period, rather than to the initial value at 120 ky BP (nominally zero). While this effect is unintentional, we inadverently thus account for the present-day survival of the Greenland ice sheet as a relic of the last glaciation – the latest evidence suggests that the Greenland ice sheet was much reduced during the last interglacial (116–130 ky BP), contributing up to 3.4 m of Eemian high stand of sea level (Otto-Bliesner et al., 2006).

We use a simple linear relationship to convert $\delta^{18}O_{water}$ to $\delta^{18}O_{calcite}$, according to changes in ambient temperature:

$$\delta^{18}O_{calcite}(t) = \delta^{18}O_{water}(t) - 0.25 \times [T(t) - T_{init}] \quad (3)$$

where $T(t)$ is the temperature at time t and T_{init} is the initial (120 ky BP) temperature. By this relationship, $\delta^{18}O_{calcite}$ is elevated above $\delta^{18}O_{water}$ at anomalously low temperatures as calcifiers incorporate relatively more ^{18}O into their shells. Figure 11 shows corresponding time series of deep and surface temperature at the three sites.

At the Iberian Margin core site, deep temperatures vary in the ranges –0.7 to 2.8°C (with traceable parameters) and 0.1 to 5.1°C (with subjective parameters), with minimum and maximum values reached at the LGM and in the late Holocene respectively. The impact of MWP events at the Iberian Margin is pronounced, with millennial fluctuations of around 1.5°C (traceable parameters) and 2°C (subjective parameters). These fluctuations are characterised as warm events, due to the interrupted sinking of relatively cold and salty NADW. As the overturning circulation stagnates, deep waters warm through vertical heat diffusion.

At the Bouvet Island core site, surface temperatures vary in the ranges from –1.8°C (the freezing point for seawater) to YD maxima of 1.0°C (traceable parameters) or 2.0°C (subjective parameters), with minimum values dominant over 18–70 ky BP. Clearly the Bouvet Island core site (see Fig. 1) is sufficiently far south to be periodically affected by the equatorward expansion of Antarctic sea ice throughout much of Marine Isotope Stage 3. The impact of MWP events at the Bouvet Island site is similar to that seen at the Iberian Margin. Millennial-timescale warming events of 1–2°C are a signature of the bipolar seesaw in temperature (Stocker and Johnsen, 2003) associated with an interruption of northward heat transport in the South Atlantic.

At the Chatham Rise core site, surface temperatures vary in the ranges 8.0 to 12.4°C (with traceable parameters) and 11.5 to 15.0°C (with subjective parameters), with minimum and maximum values reached at the LGM and in both interglacials respectively. This core site, just south of New Zealand (see Fig. 1), is located equatorward of the subantarctic front, during both interglacial and glacial climate. As a consequence, surface temperatures are substantially higher than at Bouvet Island. As in the case of minimum Pacific overturning rates, very little MWP-forced variability is evident in the South Pacific.

Simulated modern temperatures are realistic: deep temperatures are close to hydrographic measurements at the Iberian Margin site (e.g. Fig. 2a of Álvarez et al., 2004), and surface temperatures are close to climatological values at the Bouvet Island and Chatham Rise sites. The ocean is notably warmer at all three sites in experiment MWP-1s (subjective parameters), compared with experiment MWP-1t (traceable parameters). This contrasts with lower high-latitude air temperatures in MWP-1s (compared to MWP-1t) – see Fig. 6. This can be understood in the context of an ocean-atmosphere heat balance: in the mid and high latitudes of MWP-1s, more heat is stored in the ocean and less heat is stored in the atmosphere, compared to MWP-1t.

Using Eq. (3) with the $\delta^{18}O_{water}$ and temperature data in Figs. 10 and 11, we obtain the simulated time series of $\delta^{18}O_{calcite}$ variations, shown in Fig. 12 (red, green, light blue and dark blue curves), which can be directly compared with the core measurements (black curves). As with $\delta^{18}O_{water}$ (Fig. 10) the broad glacial-interglacial variation in $\delta^{18}O_{calcite}$ is reproduced in Fig. 12, although the adjustment of $\delta^{18}O_{water}$ to account for temperature effects now subtly modifies the shape of the curves, improving agreement with the measured $\delta^{18}O_{calcite}$ records. For example, the record of $\delta^{18}O_{water}$ at the Iberian Margin simulated in MWP-3 (dark blue curve in Fig. 10a) features a primary peak at 60 ky BP and a secondary peak at the LGM, while measured $\delta^{18}O_{calcite}$ has a primary peak at the LGM and a secondary peak around 60 ky BP. However, temperatures at the LGM are around 1.5°C lower than around 60 ky BP (Fig. 11a), so by accounting for the temperature effect, we capture the primary LGM peak in $\delta^{18}O_{calcite}$.

The "LGM minus Present Day" difference in simulated $\delta^{18}O_{calcite}$ largely matches that seen in the core measurements of $\delta^{18}O_{calcite}$ at all three sites. However, at the Iberian Margin the LGM peak in simulated $\delta^{18}O_{calcite}$ at 20 ky BP precedes the peak in measured $\delta^{18}O_{calcite}$ by 3000 years. As simulated $\delta^{18}O_{calcite}$ is strongly linked to the onset of specified deglaciation meltwater flux, it would be reasonable to assume that this should in fact start at around 17 ky BP in the North Atlantic. The high frequency of millennial variability seen in the measured records of $\delta^{18}O_{calcite}$ is not reproduced in the simulated records. It is likely that much of this observed variability is associated

with internal variability of the climate system (rather than external forcing), behaviour that cannot be simulated with the simplified atmosphere in the GENIE-1 model. However, some multi-millennial variability is captured through MWP forcing, and on visual inspection of the curves in Fig. 12 there is a degree of agreement between model and observations. In particular, secondary maxima in $\delta^{18}O_{calcite}$ at 60–70 ky BP are simulated in MWP-3. These features, at all three sites, are a global signal associated with extensive glaciation prior to around 65 ky BP, which is only specified when we include extra MWPs in the southern hemisphere.

To objectively compare the degree of agreement between simulated and measured $\delta^{18}O_{calcite}$ at the three core sites, we calculate correlation coefficients over the full simulation period 0–120 ky BP, and over the shorter 10–65 ky BP period which includes the last deglaciation and Marine Isotope Stage 3 – see Table 3. We select the latter period as the simulated $\delta^{18}O_{calcite}$ record in experiment MWP-3 appears to be strongly influenced by the six Antarctic MWPs between 14.5 and 60 ky BP. Correlations are in all cases high and significant, as the simulated time series are strongly constrained by boundary conditions. The very high correlations at Bouvet Island are somewhat misleading due to the relative paucity of measurements prior to 60 ky BP.

Correlations for the Iberian Margin site are of particular interest. Lower correlations in MWP-1s (r=0.65) compared to MWP-1t (r=0.73) are principally associated with differences over the deglaciation. Although we prefer the subjective parameter set over the traceable parameter set on the basis that the Atlantic overturning collapses throughout the deglaciation with the latter, our prescribed MWP forcing through this period is clearly problematic. Nevertheless, considering the progression from MWP-1s to MWP-2 and MWP-3, we clearly obtain improvements in correlation through refinement of MWP forcing (using the same parameter set). In particular, the prescription of MWP forcing in the southern hemisphere leads to improvements in the simulation of Iberian Margin $\delta^{18}O_{calcite}$ over 10–65 ky BP (an increase of correlation coefficient from 0.50 to 0.60). However, prescribed southern hemisphere MWPs reduce the same correlation coefficient at Chatham Rise, from 0.86 to 0.74. This suggests that our prescription of

circumpolar MWPs in the southern hemisphere is naïve, and that the majority of melt water may have entered the Southern Ocean more locally, perhaps through periodic break-up of the West Antarctic Ice Sheet. Under such a scenario, $\delta^{18}O_{calcite}$ excursions would be stronger in the Atlantic sector and weaker in the Pacific sector.

5 Conclusions

Calcite $\delta^{18}O$ measurements in cores around the World Ocean reveal glacial-interglacial changes in both ice sheets and climate, strongly influenced by Meltwater Pulses (MWPs), highly uncertain in location, timing and magnitude. Large MWPs are otherwise known as Heinrich events, based on layers of ice rafted debris (IRD) identified in sediment cores obtained in the North Atlantic (Heinrich, 1988). Evidence for IRD/meltwater events has also been identified in cores recovered from the Southern Ocean (Kanfoush et al., 2000). A low-resolution EMIC forced by changing boundary conditions and a range of plausible MWPs in both hemispheres has been used to simulate changes in the oceanic thermohaline circulation, climate and oxygen isotopes in the ocean over the last 120 000 years. Even at low resolution, it takes several days to complete one such experiment, and so only a limited number of experiments have been undertaken. Results are sensitive to model parameter set. Initially comparing simulations with the "subjective" and "traceable" parameter sets previously developed for GENIE-1 (Lenton et al. 2006), we find that the former provides better agreement with high latitude temperature reconstructions and a more realistic modern-day global thermohaline circulation, and is subsequently used in further MWP sensitivity experiments.

Our aspiration was to reproduce the $\delta^{18}O$ in calcite records obtained from three sediment cores. The overall good agreement between synthetic and measured calcite $\delta^{18}O$ records is largely due to heavily prescribed boundary conditions, although subtle differences between the three MWP sensitivity experiments are instructive. In particular, we obtain substantially better agreement with the Iberian Margin record when using a sce-

nario comprising variable-strength Heinrich events (rather than nine identical-strength events) plus MWPs around Antarctica. This result supports both the evidence reviewed by Hemming (2004) for two different types or classes of Heinrich event, and the assertion of Rohling et al. (2004) that Antarctic ice sheets may have contributed substantially to glacial sea-level variability. The simulated calcite $\delta^{18}O$ record at the Iberian margin does not reproduce the multi-millennial variability during Marine Isotope Stage 3 that closely matches proxies for Antarctic surface temperature (Shackleton et al., 2000). This may be because isotopic fractionation on phase changes in the hydrological cycle is not included in GENIE-1. However, we do concur with the hypothesis of Shackleton et al. (2000) that a combination of changes in ice volume and water temperature accounts for the higher frequency variations in this record, and we propose an extension of that hypothesis to invoke the important contribution of substantial changes in Antarctic ice volume, particularly during Marine Isotope Stage 3 for which we identify five MWP events of southern origin.

For better agreement between simulated and measured $\delta^{18}O$, several model improvements are essential. It is desirable to incorporate wind fields that are consistent with the slowly changing boundary conditions, allowing atmospheric moisture transport to vary likewise. Furthermore, better resolution of high latitude processes, particularly deep water formation, would increase our confidence in the response of the thermohaline circulation to MWP forcing. Also necessary is explicit representation of $^{16}O/^{18}O$ fractionation caused by both physical (evaporation/condensation) and biological (calcification) processes. We are also now in a position to add fidelity to our MWP forcing. For example, in the North Atlantic we can specify the iceberg fluxes predicted by an ice sheet model (e.g. Marshall and Koutnik, 2006). Furthermore, we can specify alternative routing of meltwater from the northern ice sheets, according to a range of published hypothesis (see Broecker, 2006). Finally, there remains the technical challenge of altering the land-sea mask and ocean topography, according to reconstructions of paleogeography, during long transient experiments. This could be undertaken by running a series of shorter sequential experiments, perhaps of millennial length, in

which the land-sea mask and topography are updated at the start of each experiment, ensuring conservation of total heat and freshwater content on re-partitioning oceanic heat and freshwater between atmosphere, sea ice, and land (principally ice sheets). All of these improvements and enhancements are planned for future experiments with GENIE models. The present study has provided strong guidance for such experiments.

Acknowledgements. The UK Natural Environment Research Council (NERC) funded the GENIE (NER/T/S/2002/00217) and ongoing GENIEfy (NE/C515904) projects through its e-Science directed programme. RM is supported under NERC Core Strategic Research Programmes at NOC. Research of EJR is supported by the NERC Rapid Climate Change Directed Programme. This study is a preliminary study in support of the NERC Directed Programme Quantifying and Understanding the Earth System (QUEST). We thank M. Siddall for discussions on proxy records of glacial-interglacial sea level.

References

Alley, R. B. and Clark, P. U.: The glaciation of the northern hemisphere: a global perspective, Ann. Rev. Earth Planet. Sci., 27, 149–182, 1999.

Alley, R., Anandakrishnan, S., and Jung, P.: Stochastic resonance in the North Atlantic, Paleoceanography, 16, 190–198, 2001.

Alley, R. B.: GISP2 Ice Core Temperature and Accumulation Data, IGBP PAGES/World Data Center for Paleoclimatology Data Contribution Series #2004-013. NOAA/NGDC Paleoclimatology Program, Boulder CO, USA, 2004.

Álvarez, M., Pérez, Bryden, H. L., and Ríos, F. F.: Physical and biogeochemical transports structure in the North Atlantic subpolar gyre, J. Geophys. Res., 109, C03027, doi:10.1029/2003JC002015, 2004.

Anderson, J. B., Shipp, S. S., Lowe, A. L., Wellner, J. S., and Mosola, A. B.: The Antarctic Ice Sheet during the Last Glacial Maximum and its subsequent retreat history: a review, Quat. Sci. Rev., 21, 49–70, 2002.

Andrews, J. T., Erlenkeuser, H., Tedesco, K., Aksu, A. E., and Jull, A. J. T.: Late Quaternary (stage 2 and 3) meltwater and Heinrich events, northwest Labrador Sea, Quat. Res., 41, 26–34, 1994.

Arnold, N. S., van Andel, T. H., and Valen, V.: Extent and dynamics of the Scandanavian ice sheet during Oxygen Isotope Stage 3 (60 000–30 000 yr BP), Quat. Res., 57, 38–48, 2000.

Bard, E., Hamelin, B., Arnold, M., Montaggioni, L., Cabioch, G., Faure G., and Rougerie, F.: Deglacial sea-level record from Tahiti corals and the timing of global meltwater discharge, Nature, 241, 382, 1996.

Berger, A. L.: Long-term variations of daily insolation and Quaternary climatic changes, J. Atmos. Sci., 35, 2362–2367, 1978.

Blunier, T., Chappellaz, J., Schwander, J., Dallenbach, A., Stauffer, B., Stocker, T. F., Raynaud, D., Jouzel, J., Clausen, H. B., Hammer, C. U., and Johnsen, S. J.: Asynchrony of Antarctic and Greenland climate change during the last glacial period, Nature, 394, 739–743, 1998.

Bond, G., Heinrich, H., Broecker, W., Labeyrie, L., Mcmanus, J., Andrews, J., Huon, S., Jantschik, R., Clasen, S., Simet, C., Tedesco, K., Klas, M., Bonani, G., and Ivy, S.: Evidence for massive discharges of icebergs into the North Atlantic ocean during the last glacial, Nature, 360, 245–249, 1992.

Bond, G. C., Broecker, W. S., Johnsen, S., McManus, J. F., Labeyrie, L., Jouzel, J., and Bonani, G.: Correlation between climate records from North Atlantic sediments and Greenland ice, Nature, 365, 143–147, 1993.

Bond, G. C. and Lotti, R.: Iceberg discharges into the North Atlantic on millennial time scales during the last deglaciation, Science, 267, 1005–1010, 1995.

Broecker, W. S., Peteet, D. M., and D. Rind: Does the ocean–atmosphere system have more than one stable mode of operation?, Nature, 315, 21–26, 1985.

Broecker, W. S., Andree, M., Wolli, W., Oeschger, H., Bonani, G., Kennett, G., and Peteet, D.: A case in support of a meltwater diversion as a trigger for the onset of the younger dryas, Paleoceanography, 3, 1–19, 1988.

Broecker, W. S., Bond, G. C., Klas, M., Clark, E., and McManus, J. F.: Origin of the northern Atlantic's Heinrich events, Clim. Dyn., 6, 265–273, 1992.

Broecker, W. S.: Abrupt climate change:causal constraints provided by the paleoclimate record, Earth Sci. Rev. 51, 137–154, 2000.

Broecker, W. S.: Was the Younger Dryas Triggered by a Flood?, Science, 312, 1146–1148, 2006.

Chapman, M. R. and Shackleton, N. J.: Millennial-scale fluctuations in North Atlantic heat flux during the last 150 000 years, Earth Planet. Sci. Lett., 159, 57–70, 1998.

Clark, P. U. and Mix, A. C.: Ice sheets and sea level of the Last Glacial Maximum, Quat. Sci.

Rev., 21, 1–7, 2002.
Clark, P. U., Pisias, N. G., Stocker, T. F., and Weaver, A. J.: The role of the thermohaline circulation in abrupt climate change, Nature, 415, 863–869, 2002.
Claussen, M., Mysak, L., Weaver, A., Crucifix, M., Fichefet T., Loutre, M., Weber, S., Alcamo, J., Alexeev, V., Berger, A., Calov, R., Ganopolski, A.,Goosse,. H, Lohmann, G., Lunkeit, F., Mokhov, I., Petoukhov, V., Stone, P., and Wang, Z.: Earth system models of intermediate complexity:closing the gap in the spectrum of climate system models, Clim. Dyn., 18, 579–586, 2002.
Cutler, K. B., Edwards, R. L., Taylor, F. W., Cheng, H., Adkins, J., Gallup, C. D., Cutler, P. M., Burr, G. S., and Bloom, A. L.: Rapid sea-level fall and deep-ocean temperature change since the last interglacial period, Earth Planet. Sci. Lett., 206, 253–271, 2003.
Dansgaard, W., Johnsen, S. J., Clausen, H. B., Dahljensen, D., Gundestrup, N. S., Hammer, C. U., Hvidberg, C. S., Steffensen, J. P., Sveinbjornsdottir, A. E., Jouzel, J., and Bond, G.: Evidence for general instability of past climate from a 250-kyr ice-core record, Nature, 364, 218–220, 1993.
Delaygue, G., Jouzel, J., and Dutay, J. C.: Oxygen 18-salinity relationship simulated by an oceanic general circulation model, Earth Plan. Sci. Lett., 178, 113–123, 2000.
Dickson, R. R. and Brown, J.: The production of North Atlantic Deep Water: Sources, rates, and pathways, J. Geophys. Res., 99, 12 319–12 341, 1994.
Duplessy, J. C., Shackleton, N. J., Fairbanks, R. G., Labeyrie, L., Oppo, D., and Kallel, N.: Deepwater source variations during the last climatic cycle and their impact on the global deepwater circulation, Paleoceanography, 3, 343–360, 1988.
Edwards, N. R. and Marsh, R.: Uncertainities due to transport-parameter sensitivity in an efficient 3-D ocean-climate model, Clim. Dyn., 24, 415–433, 2005.
Fanning, A. G. and Weaver, A. J.: An atmospheric energy-moisture model: climatology, interpentadal climate change and coupling to an ocean general circulation model, J. Geophys. Res., 101, 15 111–15 128, 1996.
Flückiger, J., Knutti, R., and White, J. W. C.: Oceanic processes as potential trigger and amplifying mechanisms for Heinrich events, Paleoceanography, 21, PA2014, doi:10.1029/2005PA001204, 2006.
Gallee, H., van Ypersele, J. P., Fichesfet, T., Tricot, C., and Berger, A.: Simulation of the last glacial cycle by a coupled sectorially averaged climate – ice sheet model. 1. The climate model, J. Geophys. Res., 96, 13 139–13 161, 1991.

Ganopolski, A. and Rahmstorf, S.: Rapid changes of glacial climate simulated in a coupled climate model, Nature, 409, 153–158, 2001.
Genthon, C., Barnola, J. M., Raynaud, D., Lorius, C., Jouzel, J., Barkov, N. I., Korotkevich, Y. S., and Kotlyakov, V. M.: Vostok ice core: Climatic response to CO2 and orbital forcing changes over the last climatic cycle, Nature, 329, 414–418, 1987.
Grousset, F. E., Labeyrie, L., Sinko, J., Cremer, M., Bond, G., Duprat, J., Cortijo, E., and Huon, S.: Patterns of ice-rafted detritus in the glacial North Atlantic (40–55° N), Paleoceanography, 8, 175–192, 1993.
Grousset, F. E., Pujol, C., Labeyrie, L., Affret, G., and Boelaert, A.: Were the North Atlantic Heinrich events triggered by the behaviour of the European ice sheets?, Geology, 28, 123–126, 2000.
Gwiazda, R. H., Hemming, S. R., Broecker, W. S., Onsttot, T., and Mueller, C.: Evidence from Ar-40/Ar-39 ages for a Churchill province source of ice-rafted amphiboles in Heinrich layer 2, J. Glaciol., 42, 440–446, 1996.
Hargreaves, J. C., Annan, J. D., Edwards, N. R., and Marsh, R.: An efficient climate forecasting method using an intermediate complexity Earth system model and the ensemble Kalman Filter, Clim. Dyn., 23, 745–760, 2004.
Heinrich, H.: Origin and consequences of cyclic ice rafting in the northeast Atlantic Ocean during the past 130 000 years, Quat. Res., 29, 142–152, 1988.
Hemming, S. R.: Heinrich Events: Massive late Pleistocene detritus layers of the North Atlantic and their global climate imprint, Rev. Geophys., 42, 1–43, 2004.
Hewitt, C. D., Broccoli, A. J., Mitchell, J. F. B., and Stouffer, R. J.: A coupled model study of the last glacial maximum: Was part of the North Atlantic relatively warm?, Geophys. Res. Lett., 28, 1571–1574, 2001.
Hibler, W. D.: A dynamic thermodynamic sea ice model, J. Phys. Oceanogr., 9, 815–846, 1979.
Hill, H. W., Flower, B. P., Quinn, T. M., Hollander, D. J., and Guilderson, T. P.: Laurentide Ice Sheet meltwater and abrupt climate change during the last glaciation, Paleoceanography, 21, PA1006, doi:10.1029/2005PA001186, 2006.
Jouzel, J., Russell, G. L., Suozzo, R. J., Koster, R. D., White, J. W. C., and Broecker, W. S.: Simulations of HDO and H218O atmospheric cycles using the NASA GISS general circulation model: The seasonal cycle for present-day conditions, J. Geophys. Res., 92, 14 739–14 760, 1987.
Jouzel, J., Barkov, N. I., Barnola, J. M., Bender, M., Chappellaz, J., Genthon, C., Kotlyakov,

V. M., Lipenkov, V., Lorius, C., Petit, J. R., Raynaud, D., Raisbeck, G., Ritz, C., Sowers, T., Stievenard, M., Yiou, F., and Yiou, P. Extending the Vostok ice-core record of paleoclimate to the penultimate glacial period, Nature, 364, 407–412, 1993.

Juillet-Leclerc, A., Jouzel, J., Lebeyrie, L., and Joussame, S.: Modern and last glacial maximum sea surface O-18 derived from an Atmospheric General Circulation Model, Earth Plan. Sci. Letts., 146, 591–605, 1997.

Kanfoush, S. L., Hodell, D. A., Charles, C. D., Guilderson, T. P., Mortyn, P. G., and Ninnemann, U.S.: Millennial-scale instability of the Antarctic ice sheet during the last glaciation, Science, 288, 1815–1818, 2000.

Kanfoush, S. L., Hodell, D. A., Charles, C. D., Janecek, T. R., and Rack, F. R.: Comparison of ice-rafted debris and physical properties in ODP Site 1094 (South Atlantic) with the Vostok ice core over the last four climatic cycles, Palaeogeo., Palaeoclim., Palaeoeco., 182, 329–349, 2002.

Kitoh, A., Murakami, S., and Koide, H.: A simulation of the Last Glacial Maximum with a coupled atmosphere-ocean GCM, Geophys. Res. Lett., 28, 2221–2224, 2001.

Knutti, R., Flückiger, J., Stocker, T. F., and Timmermann, A.: Strong hemispheric coupling of glacial climate through freshwater discharge and ocean circulation, Nature, 430, 851–856, 2004.

Labeyrie, L. D., Duplessy, J. C., Duprat, J., Juilletleclerc, A., Moyes, J., Michel, E., Kallel, N., and Shackleton, N. J.: Changes in the vertical structure of the North Atlantic Ocean between glacial and modern times, Quat. Sci. Rev., 11, 401–413, 1992.

Lambeck, K. and Chappell, J.: Sea level change through the last glacial cycle, Science, 292, 679–686, 2001.

Lenton, T. M., Williamson, M. S., Edwards, N. R., Marsh, R., Price, A. R., Ridgwell, A. J., Shepherd, J. G., and the GENIE team: Millennial timescale carbon cycle and climate change in an efficient Earth system model, Clim. Dyn., 26, 687–711, 2006.

Lorius, C., Jouzel, J., Ritz, C., Merlivat, L., Barkov, N. I., Korotkevich, Y. S., and Kotlyakov, V. M.: A 150 000-year climatic record from Antarctic ice, Nature, 316, 591–596, 1985.

Lunt, D. J., Williamson, M. S., Valdes, P. J., and Lenton, T. M.: Comparing transient, accelerated, and equilibrium simulations of the last 30 000 years with the GENIE-1 model, Climtate Past Discuss., 2, 267–283, 2006.

Manabe, S. and Stouffer, R. J.: Coupled ocean-atmosphere model response to freshwater input: Comparison to Younger Dryas event, Paleoceanography, 12, 321–336, 1997.

Marshall, S. J. and Koutnik, M. R.: Ice sheet action versus reaction: Distinguishing between Heinrich events and Dansgaard-Oeschger cycles in the North Atlantic, Paleoceanography, 21, PA2021, doi:10.1029/2005PA001247, 2006.

McManus, J. F., Oppo, D. W., and Cullen, J. L.: A 0.5-million-year record of millennial-scale climate variability in the North Atlantic, Science, 283, 971–975, 2004.

Milne, G. A., Mitrovica, J. X., and Schrag, D. P.: Estimating past continental ice volume from sea-level data, Quat. Sci. Rev., 21, 361–376, 2002.

Moore Jr., T. C., Walker, J. C. G., Rea, D. K., Lewis, C. F. M., Shane, L. C. K., and Smith, A. J.: Younger Dryas interval and outflow from the Laurentide ice sheet, Paleoceanography, 15, 4–18, 2000.

Otto-Bliesner, B. L., Marshall, S. J., Overpeck, J. T., Miller, G, H., Hu, A., and CAPE Last Interglacial Project members: Simulating Arctic climate warmth and icefield retreat in the last interglaciation, Science, 311, 1751–1753, 2006.

Pahnke, K., Zahn, R., Elderfield, H., and Schultz, M.: 340 000-year centennial-scale marine record of Southern Hemisphere climatic oscillation, Science, 301, 948–952, 2003.

Pälike, H.: Orbital variation (including Milankovitch Cycles): Encyclopaedia of Geology, edited by: Selley, R. C., Cocks, R. M., and P. I. R., Elsevier, Oxford), 1, 410–421, 2005.

Peltier, W. R.: Ice-age paleotopology, Science, 265, 195–201, 1994.

Peltier, W. R.: On eustatic sea level history: Last Glacial Maximum to Holocene, Quat. Sci. Rev., 21, 377–396, 2002.

Petit, J. R., Jouzel, J., Raynard, D., Barkov, N. I., Barnola, J. M., Basile, I., Bender, M., Chappellaz, J., Davis, J., Delaygue, G., Delmotte, M., Kotlyakov, V. M., Legrand, M., Lipenkov, V., Lorius, C., Ppin, L., Ritz, C., Saltzman, E., and Strievenard, M.: Climate and atmospheric history of the past 420 000 years from the Vostok ice core, Antartica, Nature, 399, 429–436, 1999.

Rahmstorf, S.: The thermohaline ocean circulation – a system with dangerous thresholds?, Climatic Change, 46, 247–256, 2000.

Rahmstorf, S.: Timing of abrupt climate change: a precise clock, Geophys. Res. Lett., 30(10), 1510, doi:10.1029/2003GL017115, 2003.

Roche, D., Paillard, D., Ganopolski, A., and Hoffmann, G.: Oceanic oxygen-18 at the present day and LGM: equilibrium simulations with a coupled complexity climate model of intermediate complexity, Earth Planet. Sci. Lett., 218, 317–330, 2004a.

Roche, D., Paillard, D., and Cortijo, E.: Constraints on the duration and freshwater release of

Heinrich event 4 through isotope modelling, Nature, 432, 379–382, 2004b.
Rohling, E. J., Fenton, M., Jorissen, F. J., Bertrand, P., Ganssen, G., and Caulet, J. P.: Magnitudes of sea-level lowstands of the past 500 000 years, Nature, 394, 162–165, 1998.
Rohling, E. J., Mayewski, P. A., and Challenor, P.: On the timing and mechanism of millennial-scale climate variability during the last glacial cycle, Clim. Dyn., 20, 257–267, 2003.
Rohling, E. J., Marsh, R., Wells, N. C., Siddall, M., and Edwards, N. R.: Similar meltwater contributions to glacial sea level changes from Antarctic and northern ice sheets, Nature, 430, 1016–1021, 2004.
Ruddiman, W. F.: Late Quaternary deposition of ice-rafted sand in the subpolar North Atlantic (lat 40 degrees to 65 degrees N), Geol. Soc. Am. Bull., 88, 1813–1827, 1977.
Sarnthein, M., Winn, K., Jung, S. J. A., Duplessy, J. C., Labeyrie, L., Erlenkeuser, H., and Ganssen, G.: Changes in east Atlantic deepwater circulation over the last 30 000 years: Eight time slice reconstructions, Paleoceanography, 9, 209–267, 1994.
Schmidt, G. A.: Oxygen-18 variations in a global ocean model, Geophys. Res. Lett., 25, 1201–1204, 1998.
Schmidt, G. A.: Forward modeling of carbonate proxy data from planktonic foraminifera using oxygen isotope tracers in a global ocean model, Paleoceanography, 14, 482–497, 1999.
Semtner, A. J.: A model for the thermodynamic growth of sea ice in numerical investigations of climate, J. Phys. Oceanogr., 6, 379–389, 1976.
Shackleton, N. J.: Oxygen isotopes, ice volume and sea level, Quat. Sci. Rev., 6, 183–190, 1987.
Shackleton, N. J., Hall, M. A., and Vincent, E.: Phase relationships between millennial-scale events 64 000–24 000 years ago, Paleoceanography, 15, 565–569, 2000.
Siddall, M., Rohling, E. J., Almogi-Labin, A., Hemleben, Ch., Meischner, D., Schmeltzer, I., and Smeed, D. A.: Sea-level fluctuations during the last glacial cycle, Nature, 423, 853–858, 2003.
Sloyan, B. M. and Rintoul, S. R.: The Southern Ocean limb of the global deep overturning circulation, J. Phys. Oceanogr., 31, 143–173, 2001.
Stocker, T. F. and Johnsen, S. J.: A minimum thermodynamic model for the bipolar seesaw, Paleoceanography, 18, PA1087, doi:10.1029/2003PA000920, 2003.
Upham, W.: The Glacial Lake Agassiz (monograph), United States Geological Survey, Washington, 1895.
Voelker, A. H. L., and workshop participants: Global distribution of centennial-scale records for

marine istope state (MIS) 3: a database, Quat. Sci. Rev., 21, 1185–1214, 2002.
Waelbroeck, C., Labeyrie, L., Michel, E., Duplessy, J. C., McManus, J. F., Lambeck, K., Balbon E., and Labracherie, M.: Sea-level and deep water temperature changes derived from benthic foraminifera isotopic records, Quat. Sci. Rev., 21, 295–305, 2002.
Weaver, A. J., Eby, M., Wiebe, E. C., Bitz, C. M., Duffy, P. B., Ewen, T. L., Fanning, A. F., Holland, M. M., MacFadyen, A., Matthews, H. D., Meissner, K. J., Saenko, O., Schmittner, A., Wang, H., and Yoshimori, M.: The UVic Earth System Climate Model: model description, climatology and applications to past present and future climates, Atmos. Ocean, 39, 361–428, 2001.
Weaver, A. J., Saenko, O. A., Clark, P. U., and Mitrovica, J. X.: Meltwater pulse 1A from Antarctica as a trigger of the Bølling-Allerød warm interval, Science, 299, 1709–1713, 2003.
Williamson, M. S., Lenton, T. M., Shepherd, J. G., and Edwards, N. R.: An Efficient Numerical Terrestrial Scheme (ENTS) for fast Earth System Modelling, Ecol. Modell., in press, doi:10.1016/j.ecolmodel.2006.05.027, 2006.
Zweck, C. and Huybrechts, P.: Modeling of the northern hemisphere ice sheets during the last glacial cycle and glaciological sensitivity, J. Geophys. Res., 110, D07103, doi:10.1029/2004JD005489, 2005.

Table 1. Model parameter values: "subjective" set are via manual tuning; "traceable" set are ensemble-mean values based on parameter tuning through data assimilation with the Ensemble Kalman Filter (Hargreaves et al., 2004).

Parameter	Notation	Value		Units
		Subjective	Traceable	
Ocean				
Isopyc. diff.	κ_h	2000	4126	$m^2\,s^{-1}$
Diapyc. diff.	κ_v	1×10^{-4}	1.81×10^{-5}	$m^2\,s^{-1}$
Friction	λ	2.5	3.43	$days^{-1}$
Wind-scale	W	2	1.67	–
Atmosphere				
T diff. amp.	κ_T	3.2×10^{6}	3.75×10^{6}	$m^2\,s^{-1}$
T diff. width	l_d	1	1.31	Radians
T diff. slope	s_d	0.1	0.07	–
q diff.	κ_q	1×10^{6}	1.75×10^{6}	$m^2\,s^{-1}$
T adv. coeff.	β_T	0	0.06	–
q adv. coeff.	β_q	0.4	0.14	–
FWF adjust.	F_a	0.32	0.28	Sv
RH threshold	$r_{\max}$	0.85	0.85	–
P timescale	τ_{pptn}	4	3.65	days
Sea-ice				
Sea-ice diff.	κ_i	2000	6249	$m^2\,s^{-1}$

695

Table 2. Chronology of MWPs according to Heinrich Events identified in the GISP2 nss ion series (Rohling et al., 2003).

Heinrich Event	Rohling Event	GISP2 age-range of Rohling Event (ky BP)	Model Adjusted Age (peak MWP) (ky BP)
H0	A	12.20–12.85	12.5
H1	b2	16.70–17.25	17
H2	d1	23.60–24.20	25
	d2	25.20–25.90	
H3	F	29.45–30.35	30
H4	K	39.40–40.05	40
H5	N	45.55–46.45	46
H6	S	60.80–61.60	60
H7	X	85.20–86.00	85
H9	Y	103.55–103.80	103

696

Table 3. Correlation coefficients between core measurements and simulated values of $\delta^{18}O_{calcite}$, over 0–120 ky BP and 10–65 ky BP. The simulated values are linearly interpolated (in time) to coincide with the measurements. Sample sizes are as follows: at the Iberian Margin, 407 (0–120 ky BP) and 272 (10–65 ky BP); at Bouvet Island, 305 (0–120 ky BP) and 199 (10–65 ky BP); at Chatham Rise, 747 (0–120 ky BP) and 394 (10–65 ky BP). All correlation coefficients are significantly different from zero.

Core site	Experiment	Correlation over 0–120 ky BP	Correlation over 10–65 ky BP
Iberian Margin	MWP-1t	0.73	0.32
	MWP-1s	0.65	0.22
	MWP-2	0.79	0.50
	MWP-3	0.79	0.60
Bouvet Island	MWP-1t	0.89	0.74
	MWP-1s	0.91	0.74
	MWP-2	0.90	0.71
	MWP-3	0.89	0.70
Chatham Rise	MWP-1t	0.81	0.88
	MWP-1s	0.79	0.87
	MWP-2	0.79	0.86
	MWP-3	0.74	0.74

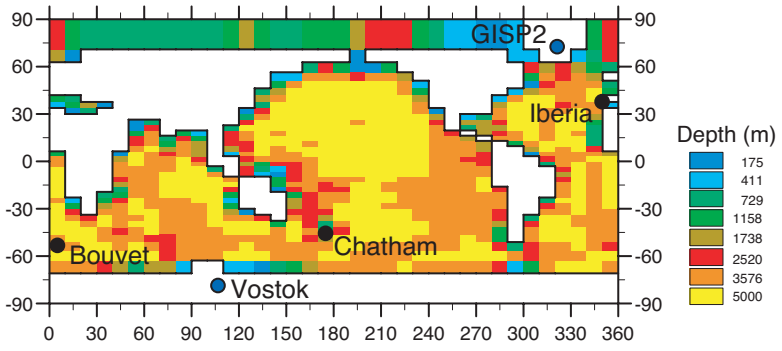

Fig. 1. Model ocean bathymetry on the GENIE-1 horizontal grid: 36×36 cells in constant increments of longitude and sin(latitude). Also indicated are the three sediment core sites (Iberian Margin, Bouvet Island, Chatham Rise – black dots) and the two ice core stations (GISP2, Vostok – blue dots).

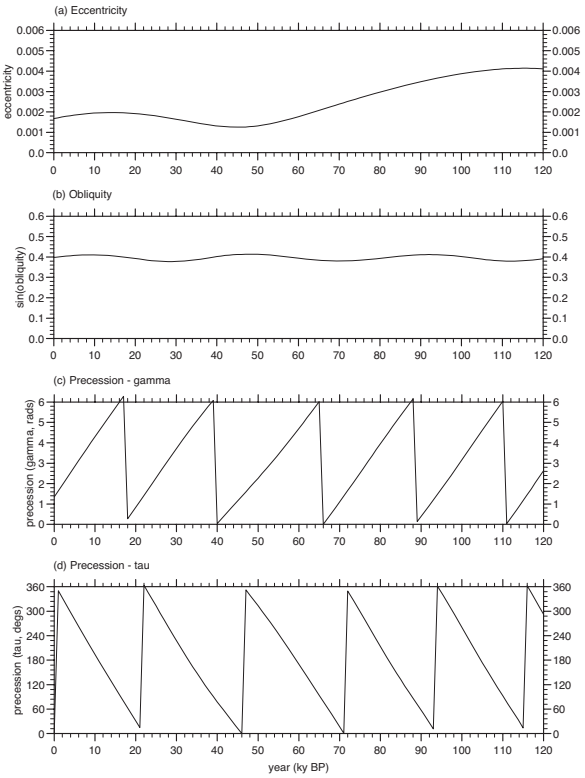

Fig. 2. Time variation of the four orbital parameters used to force GENIE-1 insolation over the last 120 000 years: **(a)** Eccentricity; **(b)** Obliquity; **(c)** and **(d)** Precession.

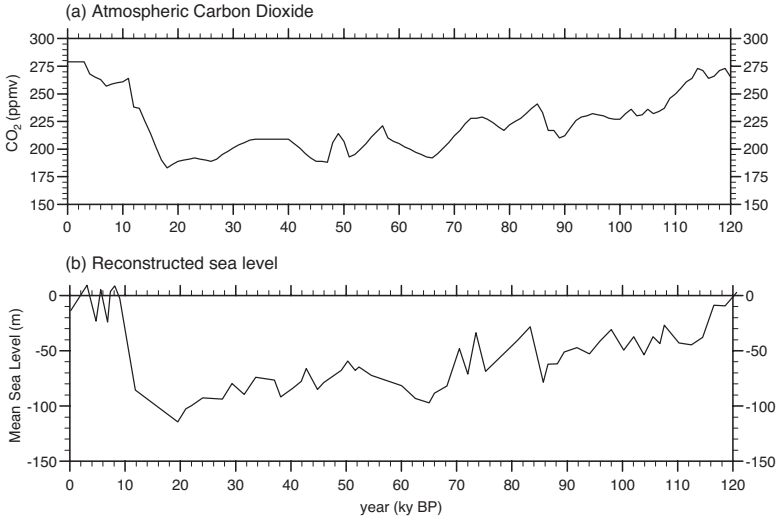

Fig. 3. Time variation over 0–120 ky BP of: **(a)** atmospheric CO_2 from air bubbles in the Vostok ice core (Petit et al., 1999); **(b)** Global mean sea level (relative to present day), as reconstructed by Siddall et al. (2003).

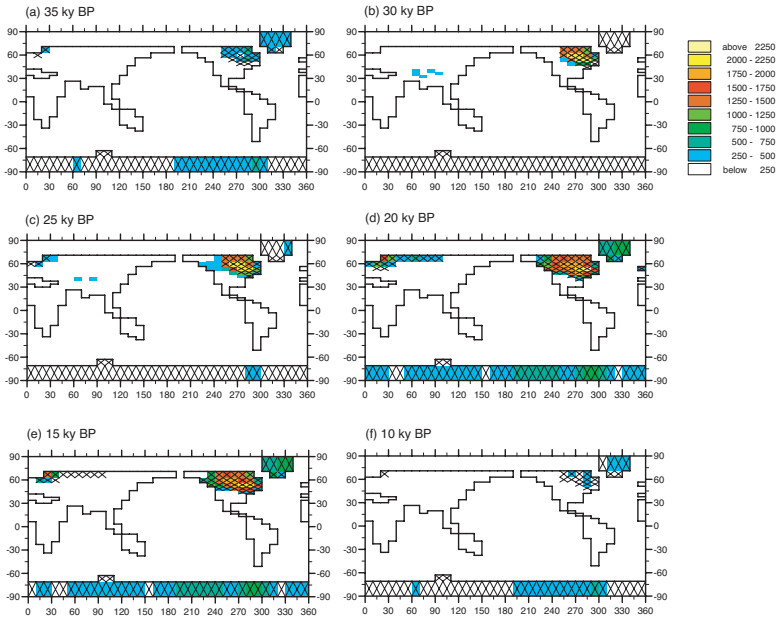

Fig. 4. Ice sheet extent (gridboxes occupied with crosses) and orography (relative to present day, colour-coded) every 5000 years for, **(a)**–**(f)**, 35 to 10 ky BP.

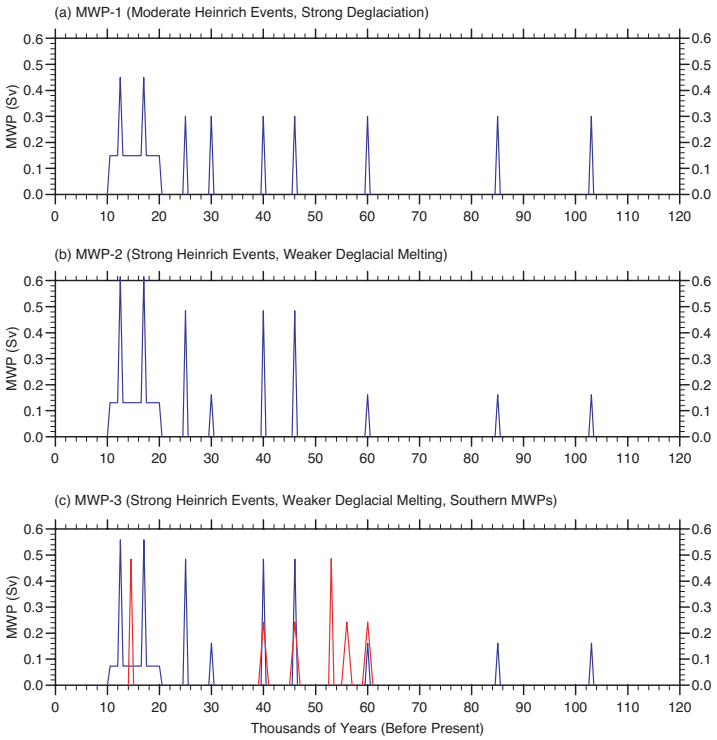

Fig. 5. Time series of Meltwater Pulses: **(a)** MWP-1; **(b)** MWP-2; **(c)** MWP-3 (see text for details). The colours identify where the MWPs are applied: blue, equally at ocean gridboxes in the Atlantic zone 50–70° N; red, equally at coastal ocean gridboxes around Antarctica.

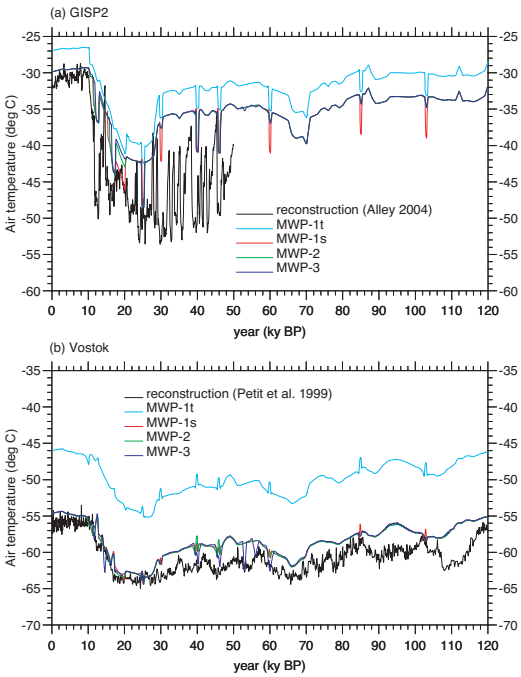

Fig. 6. Time series of annual-mean air temperature (every 100 years) inferred from ice core data and as simulated in the four GENIE-1 experiments, at two core sites: **(a)** GISP2; **(b)** Vostok.

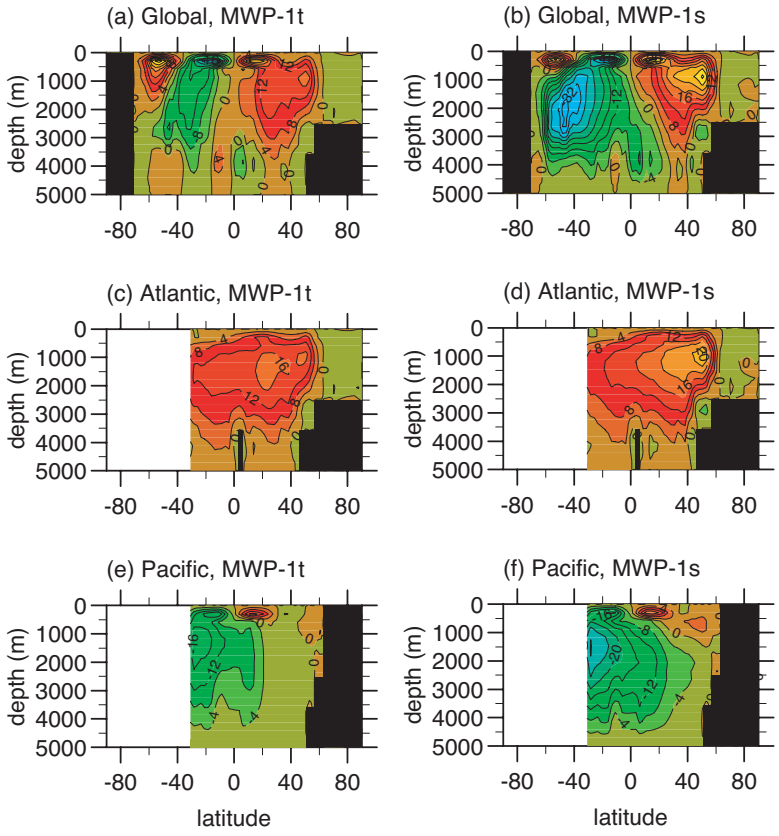

Fig. 7. Global, Atlantic and Pacific meridional streamfunctions at the end of experiments MWP-1t and MWP-1s (contour interval=4 Sv).

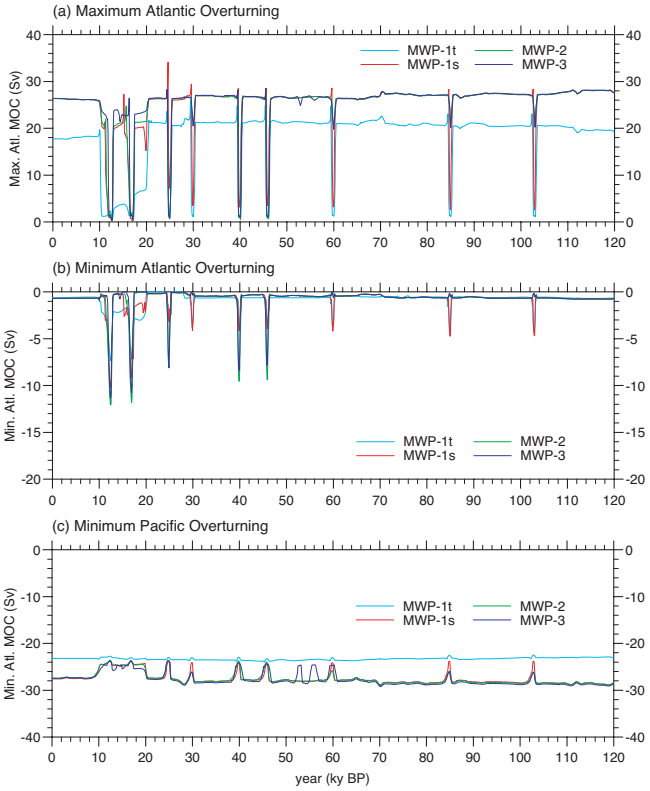

Fig. 8. Time series of: **(a)** maximum Atlantic overturning; **(b)** minimum Atlantic overturning; **(c)** minimum Pacific overturning.

705

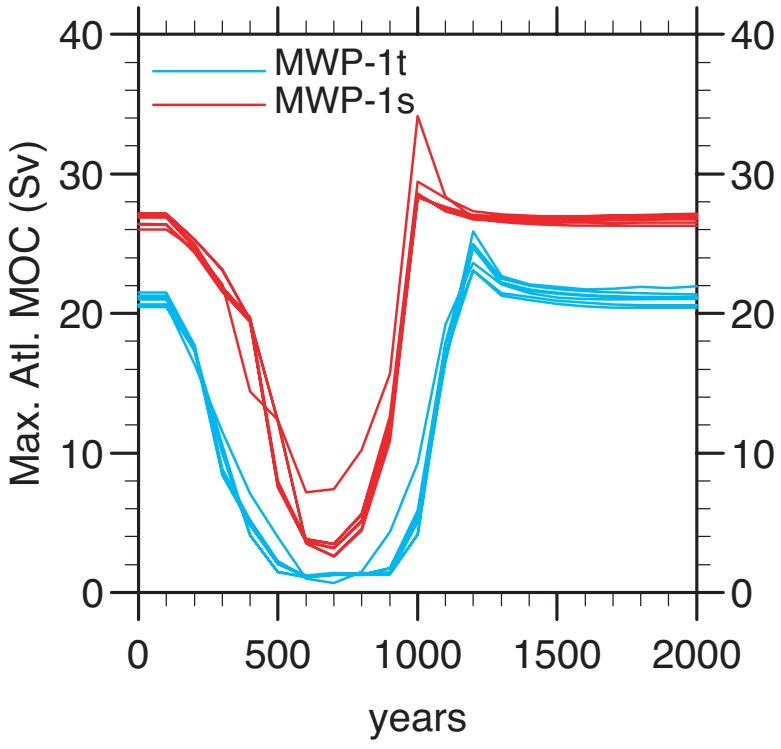

Fig. 9. Response of Atlantic overturning strength to MWP1 forcing in experiments with traceable parameter set (seven blue curves) and subjective parameter set (nine red curves).

706

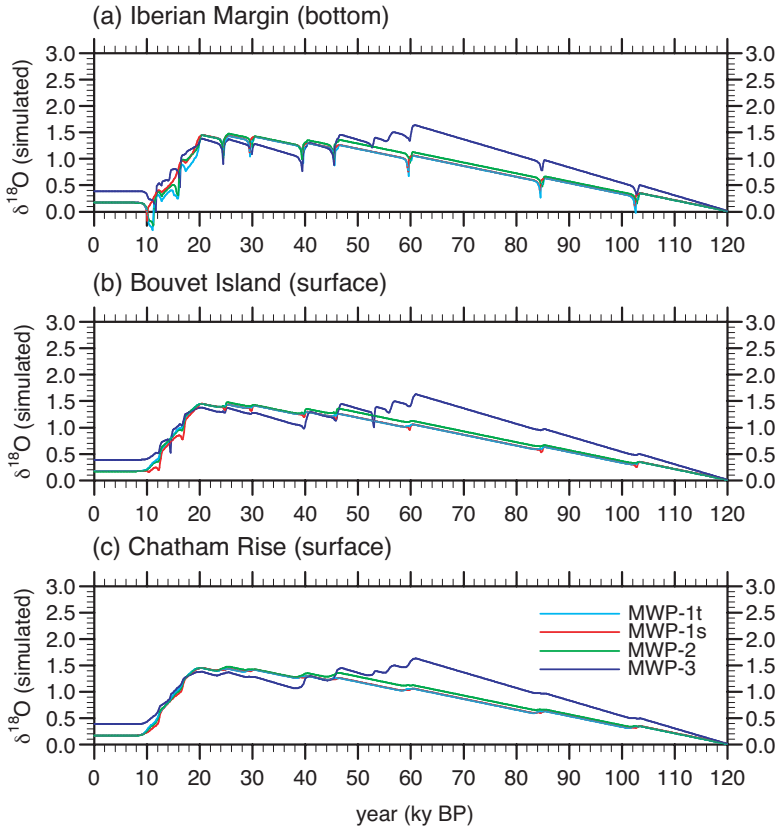

Fig. 10. Simulated $\delta^{18}O$ in water (units ppt) at: **(a)** Iberian Margin; **(b)** Bouvet Island; **(c)** Chatham Rise.

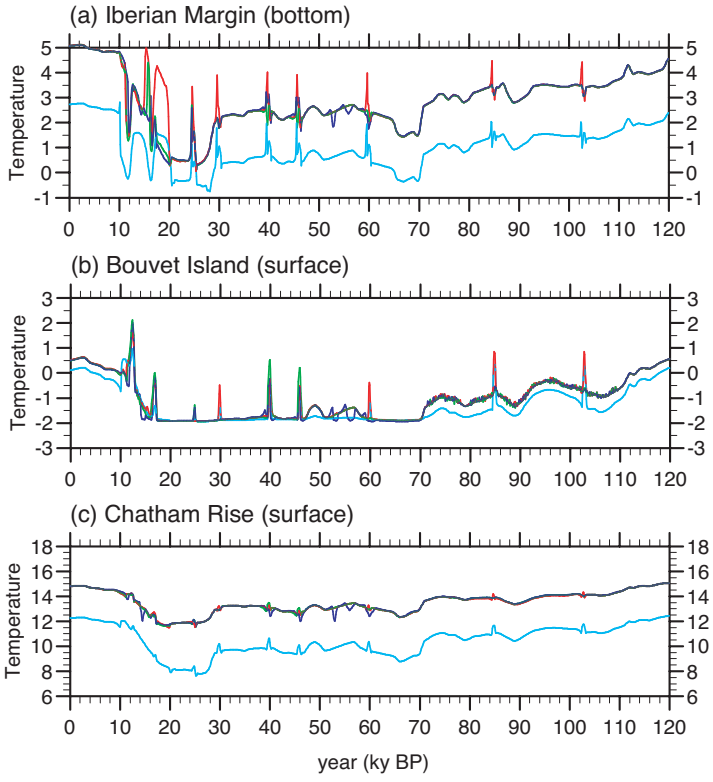

Fig. 11. Time series of temperature in gridboxes closest to sediment cores at the three sites: **(a)** Iberian Margin (bottom level); **(b)** Bouvet Island (surface level); **(c)** Chatham Rise (surface level). Colour coding as in Fig. 6.

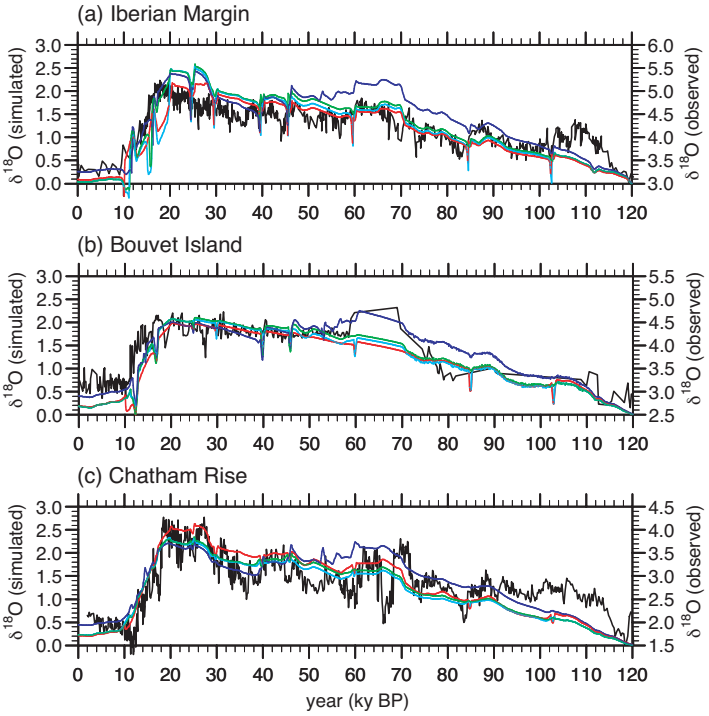

Fig. 12. Simulated and observed $\delta^{18}O$ in calcite (units ppt) at: **(a)** Iberian Margin; **(b)** Bouvet Island; **(c)** Chatham Rise. Colour coding as in Fig. 6. Note the offset of the right-hand y-axis (observed $\delta^{18}O_{calcite}$), relative to the left-hand y-axis (simulated $\delta^{18}O_{calcite}$), by +3.0 (a), +2.5 (b) and +1.5 (c).